The impact of the North Atlantic Oscillation on climate through its influence on the Atlantic Meridional Overturning Circulation

Thomas L. Delworth[1] and Fanrong Zeng[1]

[1]Geophysical Fluid Dynamics Laboratory/NOAA

201 Forrestal Rd.

Princeton, NJ 08540 USA

Submitted to Journal *of Climate*

June 4, 2015

Corresponding author: Thomas L. Delworth

E-Mail: tom.delworth@noaa.gov
Phone: 609-452-6565

Postal:
Geophysical Fluid Dynamics Laboratory/NOAA
201 Forrestal Rd.
Princeton University Forrestal Campus
Plainsboro, NJ 08540
USA

Abstract

The impact of the North Atlantic Oscillation (NAO) on the Atlantic Meridional Overturning Circulation (AMOC) and large-scale climate is assessed using simulations with three different climate models. Perturbation experiments are conducted in which a pattern of anomalous heat flux corresponding to the NAO is added to the model ocean. Differences between the perturbation experiments and a control illustrate how the model ocean and climate system respond to the NAO. A positive phase of the NAO strengthens the AMOC by extracting heat from the subpolar gyre, thereby increasing deepwater formation, horizontal density gradients, and the AMOC. The flux forcings have the spatial structure of the observed NAO, but the amplitude of the forcing varies in time with distinct periods varying from 2 to 100 years. The response of the AMOC to NAO variations is small at short time scales, but increases up to the dominant time scale of internal AMOC variability (20-30 years for the models used). The amplitude of the AMOC response, and associated oceanic heat transport, is approximately constant as the timescale of the forcing is increased further. In contrast, the response of other properties, such as hemispheric temperature or Arctic sea ice, continues to increase as the time scale of the forcing becomes progressively longer. The larger response is associated with an increased impact of radiative feedback processes at progressively longer time scales. We show that NAI fluctuations, similar in amplitude to those observed over the last century, can modulate hemispheric temperature by several tenths of a degree.

1. Introduction

One of the central challenges in climate research is to increase our ability to quantify the role of natural variability and anthropogenic forcing in observed climate change. We seek to quantify what fraction of observed changes in the climate system has come from anthropogenic and natural radiative forcing changes, and what fraction from internal variability. A key goal is therefore to improve our understanding of the mechanisms of natural climate variability, particularly on decadal and longer timescales.

Two important phenomena associated with climate variability are the North Atlantic Oscillation (NAO) and the Atlantic Meridional Overturning Circulation (AMOC). These two phenomena have been associated with a wide range of climate variations across the Northern Hemisphere on a variety of time scales (Hurrell 1995, 1996; Hurrell and Deser 2009; Trigo et al. 2002). The NAO is primarily an atmospheric phenomenon, characterized by sub-seasonal to multidecadal variations in storm tracks over the North Atlantic sector. Extensive previous work has shown that atmospheric circulation changes associated with the NAO drive an array of climate variations over North America and Europe (Scaife et al. 2008; Cullen et al. 2002; Trigo et al. 2002). These variations are clearly linked with changes in large-scale atmospheric circulation and corresponding precipitation and temperature anomalies.

The AMOC consists of a northward flow of relatively warm, salty water in the upper layers of the Atlantic, and a southward return flow at depth (Kuhlbrodt et al. 2007). The associated release of heat to the atmosphere at higher latitudes of the North Atlantic has a major impact on climate and climate variability. A rich history of modeling studies (Delworth et al. 1993; Visbeck et al. 1998; Zhu and

Jungclaus 2008; Park and Latif 2008; Biastoch et al. 2008; Vellinga and Wu 2004; Frankcombe et al. 2010; Danabasoglu et al. 2012; Medhaug et al. 2012; Menary et al. 2012; Kwon and Frankignoul 2012; Tulloch and Marshall 2012; Yeager and Danabasoglu 2012) has shown that the AMOC can have substantial variability on decadal to centennial time scales. In addition, the AMOC can have a significant influence on climate on many time scales (Delworth and Mann 2000; Knight et al. 2005; Frierson et al. 2013; Frankignoul et al. 2013). Variations in the AMOC are viewed as an important driver of the observed Atlantic Multidecadal Oscillation, which in turn influences hemispheric climate (Zhang et al. 2007; Chylek et al. 2009; Sutton and Dong 2012; Li et al. 2013; Steinman et al. 2015).

Previous work has shown a clear connection between the NAO and the AMOC (Visbeck et al. 1998; Delworth and Greatbatch 2000; Delworth and Dixon 2000; Eden and Jung 2001). Variations in the NAO have been hypothesized to play a role in AMOC variations by modifying air-sea fluxes of heat, water, and momentum. These flux variations alter vertical and horizontal density gradients in the subpolar North Atlantic, thereby inducing changes to deepwater formation and the AMOC.

In this study we examine in detail the connections between NAO variations, the AMOC, and larger scale climate through the use of large suites of climate model simulations. We design experiments to specifically examine how variations in surface fluxes associated with the NAO can induce AMOC variations, and how these AMOC variations in turn influence large-scale climate. We use model simulations to show that the AMOC influence is a function of both the timescale of the AMOC variations and the model mean state, and that the impact is hemispheric and even global in extent. We adopt a modeling framework that allows us to examine how different timescales of NAO variations influence the AMOC and the larger climate system. Our methodology involves the use of simulations

98 in which we artificially impose NAO-like fluxes on the model ocean, and assess the response of the
99 model ocean and larger-scale climate to these NAO-like variations. Using this technique we can probe
100 the response to various timescales of NAO forcing, as explained in more detail below. Recent work has
101 suggested that multidecadal NAO variations can be used as a predictor of Northern Hemispheric
102 temperature (Li et al. 2013), and in this study we conduct simulations that provide a physically based
103 underpinning for that connection.
104
105 **2. Models and experimental design**
106 **a. Models**
107 We use three versions of GFDL climate models in this study. The first is the GFDL CM2.1 model
108 (Delworth et al. 2006). This is a fully coupled ocean-atmosphere model, with land and atmospheric
109 resolution of approximately 200 Km in the horizontal, and 24 vertical levels in the atmosphere. The
110 ocean component has horizontal resolution of approximately 100 Km, with finer resolution in the
111 Tropics, and 50 levels in the vertical. This model has been used in a wide variety of studies of climate
112 variability, predictability and change, and extensive model output from past studies is available at
113 http://nomads.gfdl.noaa.gov/CM2.X/ and http://nomads.gfdl.noaa.gov:8080/DataPortal/cmip5.jsp.
114 We also use recently developed variants of this model that use considerably higher spatial resolution
115 for the atmosphere and land. These models, called FLOR and FLOR_FA (Vecchi et al. 2014), use
116 atmospheric physics that are very similar to CM2.1, but also use a much improved land model (LM3)
117 (Milly et al. 2014). The horizontal resolution of the atmosphere and land model is approximately 50
118 Km (versus 200 Km in CM2.1). The number of vertical levels in the atmosphere has increased from 24
119 in CM2.1 to 32 in FLOR and FLOR_FA. The ocean component of FLOR and FLOR_FA is very similar to
120 that in CM2.1. We have conducted a millennial-scale control simulation with each model using

radiative forcing conditions representative of "preindustrial" conditions, corresponding to approximately calendar year 1860.

The FLOR and FLOR_FA models use identical physics. The FLOR_FA model uses a technique known as "Flux Adjustment" (FA) to artificially reduce model biases (Magnusson et al. 2013). Specifically, a pattern of heat, water, and wind stress fluxes is added to the ocean component of the model to reduce the time-mean bias of the model (for example, these fluxes add heat to the model ocean surface where the model's internally generated SSTs are colder than observed). The fluxes vary seasonally, but do not change from one year to the next. The global integral of the heat and water flux adjustments is constrained to be zero so that there is no net addition or subtraction of heat or water from the system – just a horizontal redistribution of the pattern of fluxes. The fluxes are derived from preliminary simulations of the model in which the sea surface temperature (SST) is restored to time-varying, observed SSTs for the period 1971-2012 (Rayner et al. 2003). The heating associated with the restoring of SST is saved and used to calculate the flux adjustments. A similar process is used for sea surface salinity (SSS), except that the model is restored to a repeating seasonal cycle of SSS (since there are insufficient SSS observations to properly define a time-varying observational field). For wind stress, we compute the adjustment term as the difference between wind stress from the ECMWF reanalysis (Dee et al. 2011) and the model's own calculated winds in the simulation where SSTs are restored. See Vecchi et al. (2014) for further details.

b. Experimental design

We wish to assess how the model ocean responds to variations in the NAO, and then alters the rest of the climate system. In particular, we wish to study the response of the AMOC to NAO variations, and how those changes in the AMOC impact the rest of the climate system. We do this by designing

144 simulations in which the model ocean "feels" an arbitrary phase of the NAO. In these simulations we
145 intervene in the model whenever the model atmosphere and ocean exchange fluxes (described in
146 detail below). As a result, the model ocean reacts to arbitrarily imposed NAO flux anomalies. By
147 comparing the differences between simulations with and without this artificial NAO forcing, we can
148 assess how the AMOC and model climate system responds to the NAO.
149
150 We first create patterns of flux forcing that correspond to the NAO. We start with time series of
151 monthly mean surface fluxes (heat, water, momentum) from the ECMWF-Interim reanalysis (Dee et
152 al. 2011), as well as the time series of the observed NAO using a station-based index (downloaded
153 from the NCAR/UCAR climate data guide at https://climatedataguide.ucar.edu/climate-data/hurrell-
154 north-atlantic-oscillation-nao-index-station-based). We create 4-month averages over the December-
155 March period. We compute the linear regression coefficients at each grid point between the time
156 series of the reanalysis fluxes (heat, water, and momentum) and the NAO. The regression maps show
157 the pattern of surface flux anomalies that correspond to a unit change in the NAO index. In Figure 1
158 we show the regression map for surface heat flux anomalies, indicating the pattern of surface heat
159 flux change accompanying a one standard deviation increase in the NAO. For use as described below,
160 we scale the ECWMF-derived regression coefficients for the flux fields by one standard deviation of
161 the NAO index time series. We use the flux forcing only over the Atlantic from the Equator to 82^{o}N,
162 including the Barents and Nordic Seas.
163
164 The coupled models normally compute air-sea fluxes of heat, water and momentum that depend on
165 the gradients in these quantities across the air-sea interface. In our perturbation experiments this
166 process continues, but after these fluxes are calculated we add an additional flux component to the

model ocean. The model ocean therefore "feels" the fluxes that are computed based on air-sea gradients, plus an extra flux that corresponds to an arbitrary phase of the NAO. We create time series of NAO-derived fluxes that have arbitrary variations in time. In one set of experiments, referred to as "switch-on", we suddenly turn on the extra NAO flux forcing, at an arbitrary point in the control simulation, and leave these extra fluxes on with a constant amplitude corresponding to one standard deviation of the observed NAO time series. These experiments elucidate the adjustment process of the climate system in response to an instantaneous imposition of the extra NAO fluxes. We also conduct suites of experiments in which we add NAO fluxes whose amplitude is modulated sinusoidally in time with a single time scale. We conduct separate ensembles of simulations in which the NAO is modulated with periods of 2, 5, 10, 20, 50, and 100 years. These experiments assess how the response of the AMOC and climate system varies with the timescale of the NAO forcing. In all experiments the NAO forcing is applied only in the months of December through March, with a linear taper at the start and end of this period. This is the primary season of oceanic convection and deepwater formation at higher latitudes of the North Atlantic.

In order to more clearly identify the response to the NAO, all experiments are conducted as ensembles. For the CM2.1 simulations we use ten-member ensembles. The ten-members start from initial conditions that are taken from ten separate times in a long control simulation. For analysis we examine the ensemble mean of the perturbed experiments, and contrast that with the ensemble mean of the corresponding sections of the control simulation. For FLOR and FLOR_FA we use five-member ensembles, primarily because of the greater expense associated with the higher resolution models.

In our experimental design we can impose NAO-related fluxes of heat, water, or momentum. Preliminary simulations (not shown) have indicated that variations in heat flux have a dominant impact on the AMOC in these models for the decadal-scale variability being examined. Therefore, in subsequent experiments we only impose NAO-related changes in heat flux. However, it is possible that the ocean model used here does not respond as energetically to momentum fluxes as it should, possibly as a consequence of its relatively coarse resolution. Additional studies with higher resolution models that produce more energetic flow should reassess this issue. This is particularly relevant in light of the impact of observed wind stress anomalies for AMOC variability on interannual time scales (Roberts et al. 2013).

We have conducted simulations using NAO-related surface fluxes as defined both from the ECMWF-Interim reanalysis, and as evaluated from a long control integration of the CM2.1 model (pattern shown in Fig. 1b). Since the results were fairly similar when using either set of fluxes to construct the anomaly forcing, we show here only results using the reanalysis forcing. An additional benefit is that such forcings could also be used in similar experiments with other models.

3. Simulated AMOC: mean and variability

We show in Figure 2 the time-mean AMOC from control simulations of the three models. All show a robust AMOC, with substantial cross-equatorial flow. The AMOC is largest in the CM2.1 model, and weakest in FLOR_FA. All have maximum flow in the subpolar gyre of the North Atlantic. For each model we compute an index of the AMOC as the maximum value of the annual mean overturning streamfunction between 20^{o}N and 65^{o}N in the North Atlantic. We form time series of the AMOC index for each model, and then compute their spectra, shown in the bottom panel of Figure 2. All are

212 characterized by significant peaks on interdecadal time scales. The peak in CM2.1 occurs around 15-
213 20 years, around 26-30 years in FLOR, and 35-40 years in FLOR_FA. The overall variance is
214 comparable in CM2.1 and FLOR, while distinctly smaller in FLOR_FA. By performing identical
215 experiments in models with differing AMOC characteristics we hope to gain some measure of the
216 robustness of results. We do not attempt in this study to identify the factors responsible for the
217 differing AMOC characteristics in these models.
218
219 **4. Response to "switch-on" of NAO forcing**
220 As a first test we use CM2.1 to simulate the response of the AMOC and climate system to suddenly
221 turning on and maintaining an anomalous NAO flux forcing whose amplitude corresponds to one
222 standard deviation of the NAO time series. Shown in Figure 3 is the time series of the response of the
223 AMOC at 45^{o}N to the NAO heat flux forcing. The simulated AMOC adjusts over a decadal scale,
224 increasing in amplitude by several Sverdrups (Sv; 1 Sv = 10^6 m^3s^{-1}). Physically, the NAO related fluxes
225 extract heat from the subpolar gyre and Labrador Seas. This increases near-surface density, mixed
226 layer depths, the rate of deepwater formation, and horizontal density gradients. These factors tend to
227 enhance the AMOC. Note also that the AMOC response is not steady, but appears to have a quasi-
228 oscillatory component, with peaks around year 10-13 and 25-28. The characteristic time scale of
229 these variations is consistent with the time scale of internal variability in CM2.1 (15-20 years as
230 shown in in Figure 2). Thus, the processes involved with the adjustment of the AMOC to this imposed
231 forcing also appear to play a role in the dominant timescale of internal variability. The response of the
232 model to a switch on of NAO-related fluxes may be a useful way to assess the internal variability
233 timescale of a model, and to delineate some of the important processes that control that timescale.
234 This would be most relevant for models in which the NAO plays a dominant role for ocean decadal-

scale variability, and less relevant for models in which other patterns of atmospheric variability, such as the East Atlantic Pattern, are dominant for ocean decadal variability.

We show the spatial structure of this adjustment process in more detail in Figure 4. This contains the climatological mean of several quantities in the top row from a long control simulation. Subsequent rows show the time-evolving response of those quantities to the imposed NAO forcing, calculated as the ensemble mean of the simulations with the NAO forcing minus the ensemble mean of the simulations without the NAO forcing. Each row from the second row to the bottom denotes a later time after the imposition of the NAO fluxes. The sequence of panels show the adjustment of mixed layer depth, surface density, SST, SSS, and the AMOC to the NAO flux. The imposed anomalous NAO heat flux in the subpolar gyre and Labrador Sea (see Figure 1) leads to near-surface cooling and increased mixed layer depths and near-surface ocean density (see the results in the second row for Lag 3, corresponding to 3 years after the imposition of the NAO fluxes). In response to the enhanced near-surface density, convection is enhanced along with a slight strengthening of the AMOC. As we move to later times (successively lower rows in the figure) the enhanced mixed layer depths and near surface density anomalies are maintained, the AMOC continues to strengthen, and the region of the enhanced AMOC expands southward. This enhanced AMOC increases ocean heat transport (not shown), leading to positive SST and SSS anomalies throughout the subpolar gyre and portions of the Greenland-Icelandic_Norwegian (GIN) Seas. This tendency continues throughout the first decade.

5. Sensitivity of impact to timescale of forcing

a. Hemispheric time series

The "switch-on" experiment is useful in illustrating the overall response of the AMOC to NAO fluxes, but we can also probe this relationship by imposing NAO-related fluxes with well-defined timescales, and assessing how the AMOC responds to differing timescales of forcing. Specifically, we create time series of anomalous fluxes that have the spatial pattern of the NAO, but whose amplitude is modulated in time by a sine wave with arbitrary periods. We have conducted 10-member ensembles of such experiments with CM2.1 using periodicities of 2, 5, 10, 20, 50, and 100 years, and evaluated the AMOC and climate system response to these forcings. We show in Figure 5 time series of the AMOC for simulations with various timescales of NAO-related flux forcing. Also shown in each panel (red curve) is the AMOC time series that is calculated as an ensemble average from the ten corresponding segments of the control simulation. The simulations with shorter timescales of forcing are run for shorter durations. The top panels shows simulations with timescales of 2 and 5 years, in addition to the control. The NAO-induced variability of the AMOC is quite small, and is not distinguishable from the mean of the corresponding segments of the control. The middle panel shows results from forcings with periodicities of 10 and 20 years. There is a substantial increase in the response of the AMOC to the forcing, particularly for the 20-year timescale. The bottom panel shows results from forcing at timescales of 50 and 100 years. The AMOC fluctuates at the timescale of the forcing, but the amplitude is similar to that at 20 years.

We can characterize the response at each timescale by the standard deviation of the ensemble mean AMOC time series. Figure 6a shows the standard deviation of the AMOC as a function of the timescale of the forcing. It is clear that the response is small at short timescales of forcing and increases until reaching a timescale close to the characteristic internal time scale of the model AMOC variability (~20 years). The amplitude of the AMOC response does not substantially vary as we further increase the

timescale of the forcing. We show in Fig. 6b the same quantity for ocean heat transport at 23°N, and note very similar behavior.

We expect that variations in the AMOC and oceanic heat transport may influence extratropical Northern Hemisphere surface air temperature (NHSAT) and Northern Hemisphere sea ice mean thickness (NHSI). NHSAT is computed by averaging annual mean surface air temperature for all model points poleward of 23°N, and NHSI is calculated by averaging annual mean sea ice thickness poleward of 55°N. We show in Figures 6c and 6d the amplitudes of variations of NHSAT and NHSI. We note that, as was the case with the AMOC and heat transport, variations are small at short time scales and increase up to 20 years. However, in contrast to the AMOC, the amplitude of NHSAT and NHSI variations continues to increase with the timescale of the forcing, such that the amplitude of the response for NHSI at a 100 year forcing timescale is two to three times the amplitude of the response for forcing at 20 years. Why is there a continued increase in the amplitude of the NHSAT and NHSI variations when the amplitudes of the AMOC and oceanic heat transport variations are approximately constant for timescales longer than 20 years? While the ocean heat transport influences atmospheric temperature and sea ice, there is also a potentially important role for radiative feedbacks. In response to a warming of the climate system there is reduced snow cover and sea ice, thereby leading to a positive albedo feedback. This process is more effective in these models for the longer timescales of NAO forcing. At progressively longer timescales more of the cryosphere "feels" the effect of the enhanced oceanic heat transport and can respond. Shown in Figures 6e and 6f are the amplitudes of the variations of the air-sea heat flux and the net upward shortwave radiation at the top of the atmosphere (both quantities are averaged from 23°N to 90°N). The amplitude of the variations of

these terms continues to grow for timescales longer than 20 years, indicating these play an increasingly important role at longer timescales.

To more clearly illustrate these relationships we show in Figure 7 the time series of various quantities for two sets of simulations with NAO forcing timescales of 20 years (black curves) and 100 years (red curves). The responses of the AMOC and ocean heat transport have similar amplitudes for the two timescales of forcing, consistent with Figure 6. The preferred AMOC timescale of ~15-20 years is visually apparent even in the time series of the response to 100-year forcing; note how the red curve has a dominant timescale of 100 years, as determined by the forcing, but also has 15-20-year timescale variations superimposed on the 100-year timescale response (particularly in years 1-50), despite the lack of any explicit 20-year forcing.

The larger response of surface air temperature for the 100-year timescale forcing relative to the 20-year timescale forcing is apparent in Fig. 7c. The amplitude of the response is significantly larger, and the variance of the temperature response is more than three times larger for the 100-year forcing than for the 20-year forcing. Shown in Fig. 7d are similar curves for Arctic mean sea ice thickness; the variance increases by almost a factor of 5 between the 20-year forcing and the 100-year forcing, despite similar (or even smaller, see Fig. 6a and 6b) amplitudes of AMOC and oceanic heat transport variations at 100 years relative to 20 years. These results suggest that the climatic relevance of NAO-induced AMOC variations increases substantially with timescale. The larger amplitude of the temperature response at longer timescales is at least partially attributable to the greater role of feedbacks in the system. At high latitudes the cryosphere responds to the warming or cooling induced by AMOC variations, and these cryospheric changes in turn influence the amount of shortwave

radiation reflected to space, acting as a positive feedback on the system. The time series of anomalies of upward shortwave radiation at the top of the atmosphere are shown in Fig. 7e – the variance increase by a factor of 2.6 from the 20-year forcing to the 100-year forcing. This positive albedo feedback is more effective at longer timescales as progressively more of the cryosphere is altered by the NAO-induced AMOC changes, and therefore participates in the positive feedback. We also show the time series of average air-sea heat flux poleward of 23^{o}N in Fig. 7f. The variance of the air-sea heat flux time series also increases in the 100-year forcing case relative to the 20-year forcing case by a factor of 2. As the amount of sea ice varies, more open ocean is available to flux heat more effectively from the ocean to the atmosphere; since the sea ice extent is more powerfully impacted on longer timescales, this air-sea heat flux term is also stronger for longer time scales. However, this term is somewhat limited by the total anomalous heat transport in the ocean.

The above suggest that NAO-induced changes in the AMOC create changes in ocean heat transport that drive hemispheric scale variations in surface air temperature and sea ice. In addition, the effect becomes much stronger at long time scales as the feedback processes associated with changes in snow cover and sea ice can strongly amplify the changes induced directly from ocean heat transport changes.

b. Spatial patterns of response

We show in Figures 8-12 the spatial patterns of the responses to the NAO-induced AMOC variations at both time scales. The responses are computed as the linear regression of the time series of the response for each variable (forced experiment minus control) versus the time series of anomalous NAO flux forcing, and are scaled such that the values shown represent the response to a two standard

deviation NAO forcing (meant to illustrate the difference between a one standard deviation positive NAO phase and a one standard deviation negative NAO). The responses for the January-March season for both timescales of forcing are in Figures 8 and 9, and for July-September in Figure 10 and 11. These months are chosen to emphasize responses in winter and summer sea ice as well as changes in precipitation and tropical atmospheric circulation of relevance for tropical cyclone development. We show maps corresponding to the lags of maximum response in extratropical mean surface air temperature.

The NH cold season responses for the two timescales are shown in Figure 8 and 9, and show a clear sensitivity to timescale. Surface air temperature changes (Fig. 8a and 8e) show warming at high latitudes, but the warming is larger and more extensive for the 100-year forcing. In particular, the warming signal extends over most of the Eurasian continent in the 100-year forcing case, but is largely confined to oceanic regions of the North Atlantic and Arctic in the 20-year forcing case. The stronger impact of cryospheric feedbacks at the longer time scale provides a stronger and more pervasive response. The precipitation response is shown in panels b and f. There is a general increase in precipitation over the North Atlantic for both timescales in response to the generally warmer upper ocean. One exception is the notable decrease off the northeast coast of North America in the 20-year forcing case. This is associated with local cooling associated with a southward shift of the recirculation gyre (Zhang and Vallis 2007). This effect is muted at the 100-year timescale where the warming of the North Atlantic is more pervasive. The changes in sea level pressure (SLP) are shown in panels c and g. In both cases there is reduced slp over the North Atlantic, but the larger scale structure over the Northern Hemisphere differs between the two cases. In both cases the SLP pattern does not project strongly onto the NAO. Finally, the changes in 300 hPa gopotential height are shown

372 in panels d and h. The differences in the responses are dramatic. The longer time scale forcing allows
373 more of the system to warm in response to increased oceanic heat transport and positive feedbacks,
374 so that there is a broad increase in geopotential heights across much of the Northern Hemisphere,
375 creating an interhemispheric gradient. At the shorter timescale the effect is considerably smaller. The
376 sea ice changes for the JFM season are shown in Figure 9. For the 20-year forcing sea ice changes are
377 confined to the Labrador and Nordic seas, but the changes extend over the entire Arctic for the 100-
378 year forcing case.
379
380 We show in Figure 10 results for the July-September (JAS) season. The contrasts in the response of
381 surface air temperature and sea ice thickness between the two timescales of forcing is similar to the
382 winter season. The summer precipitation response is shown in panels b and g. Consistent with
383 previous work the stronger AMOC leads to a northward migration of the Intertropical Convergence
384 Zone (ITCZ) and associated rainfall, particularly over the African/Atlantic sector. This effect is
385 considerably stronger in response to the 100-year forcing. For sea level pressure there is more
386 consistency in the responses between the timescales, with reduced slp over the North Atlantic and
387 Arctic. This reduction in slp over the Atlantic is consistent with analyses of the instrumental record
388 (Sutton and Hodson 2005). Changes in 300 hPa geopotential height are shown in panels d and i – the
389 difference is striking. For the 20-year forcing there is a modest impact, but for the 100-year forcing
390 there is a widespread increase of geopotential heights over the Northern Hemisphere, extending as
391 far south as 40^{o}s. These changes in geopotential height are consistent with the changes in the vertical
392 shear of the zonal wind (hereafter referred to as shear), shown in panels e and j. There is a dramatic
393 reduction in shear over the tropical and subtropical North Atlantic in the 100-year forcing case, with a
394 much smaller impact for the 20-year case. This suggests that NAO-induced AMOC changes would

substantially influence tropical storm activity for the 100-year forcing case, although the model used for this study does not have sufficient resolution to explicitly simulate tropical storms.

The sea ice response for JAS is shown in Figure 11. While there is very little impact for the 20-year forcing case, there is a pan-Arctic reduction in sea ice thickness for the 100-year forcing case.

We show in Figure 12 the changes in sea level height induced by the NAO forcing. As shown previously, the AMOC increases in response to positive NAO forcing; this is consistent with an enhanced zonal gradient in sea level height, with negative anomalies along the North American coast and positive anomalies in the mid-Atlantic. These results suggest that decadal scale variations in the NAO induce decadal-scale sea level changes (Goddard et al. 2015; McCarthy et al. 2015) along portions of the eastern coast of North America, with short term trends in sea level change of up to 10 cm per decade. Note that sea level heights along the east coast of North America tend to fall in response to a sustained positive NAO, and rise in response to a sustained negative NAO. This process can therefore contribute substantially to local decadal-scale sea level variations. Additional analyses show that the pattern of sea level height changes propagates to the southwest, more rapidly with the 20-year NAO forcing than the 100-year NAO forcing. The amplitude of the sea level changes is similar for the 20-year and 100-year forcing cases, consistent with similar changes in the AMOC for the two forcing cases. In terms of rates of change in sea level, this implies that the 20-year forcing would have a much greater impact on decadal-scale changes in sea level than the 100-year forcing. Their spatial structures differ somewhat, with more of the changes extending through the Labrador Sea and into Baffin Bay for the 100-year forcing. Both patterns, however, are consistent with modulation of the zonal gradient of sea level consistent with AMOC variations.

6. Sensitivity of impact to model and mean base state

The previous sections examined how the response of the AMOC and larger-scale climate to NAO variations depends on the time scale of the NAO forcing using a single model (CM2.1). In this section we explore how the response to NAO forcing depends on the model's characteristics, including its mean state. We make use of two additional models, FLOR and FLOR_FA, as described in section 2a. For all three models we conduct "switch-on" experiments in which heat fluxes corresponding to a positive phase of the NAO are suddenly applied to the model ocean. These simulations are 60 years in duration, with the anomalous flux forcing held constant (but applied only in the months of December-March). Using this simple model design we wish to compare the AMOC and climatic responses among the three models. We conduct 10-member ensembles for CM2.1, and 5-member ensembles for FLOR and FLOR_FA (we use smaller ensembles for FLOR and FLOR_FA due to the greater computational cost of the higher-resolution models).

We show in Figure 13 the AMOC and surface air temperature responses for the three models. All have an increase in AMOC and zonal mean surface air temperature in response to the switch on of the NAO forcing, but there are differences in the time scale and amplitude of the response. The results from CM2.1 and FLOR are broadly similar in amplitude, with some differences in the timescales of the response. In the adjustment of the AMOC in CM2.1 to the imposed forcing, we see not only an increase of the AMOC but a tendency to fluctuate on a 15-20-year timescale, consistent with the preferred time scale of internal variability of the model (see also Fig. 3). For FLOR the timescale of preferred internal variability is somewhat longer (Fig. 2d), and the somewhat more widely spaced "pulses" of enhanced AMOC during the adjustment process to the NAO fluxes are consistent with this longer timescale of

variability. There also appears to be a slower propagation of AMOC-related changes from high latitudes to lower latitudes in FLOR than in CM2.1, as indicated by the greater tilt of the AMOC anomalies in Figure 12b. The overall amplitude of the temperature response is somewhat larger in FLOR than CM2.1, possibly related to the thicker and more extensive sea ice in the climatological mean state of FLOR (not shown), especially in the Labrador, Nordic and Barents seas. This offers the potential for greater albedo feedback and temperature response. The response in the FLOR_FA model is smallest in amplitude for both the AMOC and surface air temperature. The reasons for the smaller response of the AMOC are not clear. There is some sampling uncertainty, and this may play a role. It is also not clear if the presence of the flux adjustments themselves impacts the model response to the NAO fluxes and thus the AMOC response. This is the subject of future work. The FLOR_FA model also has a smaller response in terms of surface air temperature. In addition to the smaller AMOC response, this could also be related to a smaller area of sea ice coverage in this model relative to the other two models, thereby reducing the impact of albedo feedback.

We also compare the models in their response to a periodic NAO forcing. We select a timescale of 50 years NAO forcing for the comparison. Based on the results of the previous section the response at 20-year forcing was somewhat muted and therefore not a good choice for the comparison. In addition, the computational cost of performing 100-year forcing experiments was substantial for the higher resolution FLOR and FLOR_FA models, so we choose to do the comparison at the intermediate time scale of 50 years.

We show in Figure 14 responses for the AMOC, ocean heat transport, and surface air temperature. The results show broad similarities between the models, with differences in the details of the

amplitude and characteristics of the response. The AMOC response is broadly similar between CM2.1 and FLOR, although the CM2.1 model response at this timescale is more limited in duration than in FLOR. The shorter internal timescale for the AMOC in CM2.1 suggests that negative feedbacks associated with the oscillatory behavior kick in more rapidly, limiting the response of the AMOC in each phase of the NAO forcing. The response in FLOR to the same forcing is more persistent, consistent with the longer timescale of internal variability. The AMOC response in FLOR_FA is more muted, consistent with previous results. The surface air temperature results are consistent with the AMOC results, with perhaps somewhat more noise in the responses (compare the temperature response in CM2.1 and FLOR to their respective AMOC responses, and it is apparent that the temperature response has more noise). The temperature response in the FLOR_FA case is even less coherent for this example.

Given this spread among the models in their response to the NAO forcing, particularly for temperature, we compute a multi-model mean response to the NAO forcing, and show this in Figure 15. We see a well-defined and coherent AMOC response to the NAO forcing, with a response amplitude of approximately 2 Sv (corresponding to a 1 standard deviation change in the NAO). This corresponds to an approximately 0.2K amplitude response of extratropical NH mean surface air temperature to a one standard deviation change in the NAO. For a 50-year timescale of forcing, this implies a trend in extratropical hemispheric temperature of 0.4K/25 years.

7. Summary and Discussion

This work systematically explores the impact of interannual to centennial scale variations in the NAO on the climate system through the effect of NAO-related surface heat fluxes on the ocean. The large-scale climatic impacts arise through NAO-induced changes to the ocean that in turn modify the rest of the climate system. We have conducted suites of experiments with multiple climate models in which we artificially impose extra heat flux anomalies on the model ocean in the North Atlantic. The heat flux anomalies have the spatial structure of the NAO, but are modified such that their areal integral is zero, meaning that there is no net addition of heat to the coupled system.

In its positive phase, NAO fluxes remove heat from the ocean in the subpolar and subtropical North Atlantic, while adding heat to the western Atlantic and eastern Nordic Seas. The removal of heat from the subpolar gyre and Labrador Sea increases near-surface density and mixed layer depths, thereby enhancing deepwater formation and horizontal density gradients, leading to an enhanced AMOC and associated poleward oceanic heat transport. By conducting simulations with multiple models in which the NAO-related fluxes are instantaneously ”switched-on” and maintained indefinitely in a positive NAO phase, we find that there is an approximate decadal-scale adjustment process in which the AMOC strengthens. This adjustment timescale varies between models, and appears to be related to the dominant timescale of unforced AMOC variability of the model.

In suites of experiments in which we subject the model to sinusoidally varying NAO-related fluxes, with periods ranging from 2 to 100 years, we see that the model AMOC has very little response to forcing at time scales shorter than a decade or so. The adjustment processes by which the AMOC responds to NAO forcing take of order a decade, so that forcing on shorter timescales is not able to significantly influence the AMOC. At longer timescales the AMOC varies largely in phase with the

509 forcing, although exhibiting some preference for forcing close to the dominant timescale of internal
510 variability (approximately 15-20 years for the CM2.1 model, and longer for the higher resolution
511 FLOR and FLOR_FA models). The amplitude of the AMOC variations are largely independent of the
512 timescale of forcing for timescales longer than 20 years. The response to NAO-like atmospheric
513 forcing has previously been studied in ocean-only models (Visbeck et al. 1998; Eden and Willebrand
514 2001; Lohmann et al. 2009), and an approximate 10 year timescale of the ocean's response to the
515 NAO has also been shown.
516
517 The large-scale climatic response to NAO-induced AMOC variations is assessed as a function of
518 timescale. While the amplitude of AMOC variations does not vary much as the timescale of forcing is
519 increased from 20 years to 100 years, the amplitude of the large-scale climatic response increases
520 substantially. While the AMOC directly influences climate through altered meridional ocean heat
521 transport and venting of that heat to the atmosphere, at longer timescales this effect is substantially
522 amplified via albedo feedbacks. At progressively longer timescales more of the cryosphere is
523 influenced by AMOC-related heat transport changes, thereby altering albedo and changing the amount
524 of shortwave radiation absorbed in the climate system. For example, the response of NH extratropical
525 surface air temperature to NAO variations of the same amplitude is three times larger for the case of
526 forcing at 100 years than at 20 years. This dependence may be a crucial factor in assessing the impact
527 of NAO-induced AMOC variations on past climates. Similar amplification can be seen in the NAO-
528 induced AMOC impacts on Artic sea ice and large-scale atmospheric circulation, including changes in
529 tropical atmospheric circulation of relevance for tropical storms.
530

We perform identical experiments with three different models in order to test the robustness of the results. We find that the primary results are robust across the models, although details of the amplitudes of the response can vary. In particular, the models have differing timescales of internal AMOC variability, and their response to a switch-on of NAO heat fluxes reflects this. The models with longer timescales of internal AMOC variability appear to respond more slowly.

These simulations focus on the response to NAO-induced surface heat flux anomalies. Preliminary experiments showed that heat flux forcing was the dominant term influencing AMOC variability in these models at longer time scales in these models. However, it should be noted that these models all use a relatively coarse ocean model, with horizontal resolution of approximately 1^{o}. The response of a model with much finer resolution and more energetic flows could be quite different, with a potentially larger sensitivity to momentum fluxes. This is especially relevant in light of the observed AMOC weakening associated with anomalous winds in 2009-2010 (Roberts et al. 2013).

Further, the impact of NAO-induced AMOC variations on the larger climate system could well be underestimated in this modeling study. The climatic impact of the AMOC will be influenced by air-sea interactions in the extratropics; these may be underestimated by many climate models in use today, including those in the present study.

The biases of the models used in this study will likely have some impact on their estimate of NAO-induced AMOC variability and its climatic impact. For example, the FLOR model has a tendency for excessive sea ice in portions of the Northern Atlantic and adjacent regions, especially in the Barents Sea. This could overestimate the impact of ice-albedo feedbacks. Similarly the albedos associated with

554 sea ice and snow cover on sea ice in CM2.1 are perhaps on the lower end of observational estimates,
555 thereby potentially underestimating ice-albedo feedbacks in CM2.1. In addition, other biases, such as
556 the displacement of the Gulf Stream and the lack of intense boundary currents and frontal zones,
557 could also have some impact on the overall estimates of variability and the sensitivity to NAO-induced
558 AMOC variability.
559
560 The amplitude of the NAO forcing used in the present study is comparable to the interdecadal-scale
561 variations observed in the NAO over the last century. Therefore, the results of this study suggest that
562 variations of the NAO could have a significant impact on the AMOC and large-scale climate over the
563 last century, including sea level in the western North Atlantic. For example, a swing of the NAO
564 corresponding to two standard deviations can alter NH extratropical surface air temperature by
565 approximately 0.4K. On sufficiently long time scales this swing would also lead to substantial changes
566 in tropical Atlantic atmospheric circulation of relevance for tropical storm formation.
567
568 One interesting aspect is that the impact of AMOC fluctuations is dependent to some extent on albedo
569 feedback. This suggests that as the climate system warms in response to increasing greenhouse gases
570 and Arctic sea ice and snow cover diminishes, the climatic impact of AMOC fluctuations would also be
571 reduced.
572
573 An important aspect of the present study is that we have employed an idealized representation of the
574 flux forcing associated with the NAO, treating the NAO as a static spatial pattern. In reality the spatial
575 characteristics of the NAO vary over time (Moore et al. 2013), and this could complicate the
576 interpretation offered by our idealized framework.

The results of this study are of course limited by the fidelity of the models employed, particularly in terms of the ocean component. The models are unable to resolve oceanic mesoscale eddies or the effects of deep overflows, such as over the sills between Greenland and Iceland, or near the Faroe Banks. The model ocean itself has relatively large viscosity, resulting in weak boundary currents and altered propagation for oceanic internal waves. In addition, the impacts of intense cyclones and their influence on air-sea interactions is missing. Nevertheless, it is likely that these models capture important relationships between the NAO, the AMOC, and larger-scale climate. These relationships are strongly influenced by oceanic adjustment to sustained changes in the NAO, involving changes in the AMOC and oceanic heat transport, and their subsequent influence on the atmosphere, including radiative feedback processes.

Acknowledgements

We wish to thank Drs. Alistair Adcroft , Yohan Ruprich-Robert, and Liping Zhang for very helpful comments on an earlier version of this manuscript.

592 **References**

593

594 Biastoch, A., C. W. Böning, J. Getzlaff, J.-M. Molines, and G. Madec, 2008: Causes of Interannual–Decadal
595 Variability in the Meridional Overturning Circulation of the Midlatitude North Atlantic Ocean. *J.*
596 *Clim.*, **21**, 6599–6615, doi:10.1175/2008JCLI2404.1.

597 Chylek, P., C. K. Folland, G. Lesins, M. K. Dubey, and M. Wang, 2009: Arctic air temperature change
598 amplification and the Atlantic Multidecadal Oscillation. *Geophys. Res. Lett.*, **36**,
599 doi:10.1029/2009GL038777. http://doi.wiley.com/10.1029/2009GL038777 (Accessed May
600 29, 2015).

601 Cullen, H. M., A. Kaplan, P. A. Arkin, and others, 2002: Impact of the North Atlantic Oscillation on
602 Middle Eastern climate and streamflow. *Clim. Change*, **55**, 315–338.

603 Danabasoglu, G., S. G. Yeager, Y.-O. Kwon, J. J. Tribbia, A. S. Phillips, and J. W. Hurrell, 2012: Variability
604 of the Atlantic Meridional Overturning Circulation in CCSM4. *J. Clim.*, **25**, 5153–5172,
605 doi:10.1175/JCLI-D-11-00463.1.

606 Dee, D. P., and Coauthors, 2011: The ERA-Interim reanalysis: configuration and performance of the
607 data assimilation system. *Q. J. R. Meteorol. Soc.*, **137**, 553–597, doi:10.1002/qj.828.

608 Delworth, T. L., and K. W. Dixon, 2000: Implications of the recent trend in the Arctic/North Atlantic
609 Oscillation for the North Atlantic thermohaline circulation. *J. Clim.*, **13**, 3721–3727.

610 ——, and R. J. Greatbatch, 2000: Multidecadal thermohaline circulation variability driven by
611 atmospheric surface flux forcing. *J. Clim.*, **13**, 1481–1495.

612 ——, and M. E. Mann, 2000: Observed and simulated multidecadal variability in the Northern
613 Hemisphere. *Clim. Dyn.*, **16**, 661–676.

614 ——, S. Manabe, and R. J. Stouffer, 1993: Interdecadal variations of the Thermohaline Circulation in a
615 Coupled Ocean-Atmosphere Model. *J. Clim.*, **6**, 1993–2011.

616 ——, and Coauthors, 2006: GFDL's CM2 global coupled climate models. Part I: Formulation and
617 simulation characteristics. *J. Clim.*, **19**.

618 Eden, C., and T. Jung, 2001: North Atlantic interdecadal variability: oceanic response to the North
619 Atlantic Oscillation (1865-1997). *J. Clim.*, **14**, 676–691.

620 ——, and J. Willebrand, 2001: Mechanism of interannual to decadal variability of the North Atlantic
621 circulation. *J. Clim.*, **14**, 2266–2280.

622 Frankcombe, L. M., A. von der Heydt, and H. A. Dijkstra, 2010: North Atlantic Multidecadal Climate
623 Variability: An Investigation of Dominant Time Scales and Processes. *J. Clim.*, **23**, 3626–3638,
624 doi:10.1175/2010JCLI3471.1.

625 Frankignoul, C., G. Gastineau, and Y.-O. Kwon, 2013: The Influence of the AMOC Variability on the
626 Atmosphere in CCSM3. *J. Clim.*, **26**, 9774–9790, doi:10.1175/JCLI-D-12-00862.1.

627 Frierson, D. M. W., and Coauthors, 2013: Contribution of ocean overturning circulation to tropical
628 rainfall peak in the Northern Hemisphere. *Nat. Geosci.*, **6**, 940–944, doi:10.1038/ngeo1987.

629 Goddard, P. B., J. Yin, S. M. Griffies, and S. Zhang, 2015: An extreme event of sea-level rise along the
630 Northeast coast of North America in 2009–2010. *Nat. Commun.*, **6**, 6346,
631 doi:10.1038/ncomms7346.

632 Hurrell, J., 1996: Influence of variations in extratropical wintertime teleconnections on Northern
633 Hemisphere temperature. *Geophys. Res. Lett.*, **23**, 665–668.

634 Hurrell, J. W., 1995: Decadal Trends in the North Atlantic Oscillation: Regional Temperatures and
635 Precipitation. *Science*, **269**, 676–679, doi:10.1126/science.269.5224.676.

636 ——, and C. Deser, 2009: North Atlantic climate variability: The role of the North Atlantic Oscillation.
637 *J. Mar. Syst.*, **78**, 28–41, doi:10.1016/j.jmarsys.2008.11.026.

638 Knight, J. R., R. Allan, C. K. Folland, M. Vellinga, and M. E. Mann, 2005: A signature of persistent natural
639 thermohaline circulation cycles in observed climate. *Geophys. Res. Lett.*, **32**,
640 doi:10.1029/2005GL024233. http://doi.wiley.com/10.1029/2005GL024233 (Accessed April
641 28, 2015).

642 Kuhlbrodt, T., A. Griesel, M. Montoya, A. Levermann, M. Hofmann, and S. Rahmstorf, 2007: On the
643 driving processes of the Atlantic meridional overturning circulation. *Rev. Geophys.*, **45**,
644 doi:10.1029/2004RG000166. http://doi.wiley.com/10.1029/2004RG000166 (Accessed April
645 7, 2015).

646 Kwon, Y.-O., and C. Frankignoul, 2012: Stochastically-driven multidecadal variability of the Atlantic
647 meridional overturning circulation in CCSM3. *Clim. Dyn.*, **38**, 859–876, doi:10.1007/s00382-
648 011-1040-2.

649 Li, J., C. Sun, and F.-F. Jin, 2013: NAO implicated as a predictor of Northern Hemisphere mean
650 temperature multidecadal variability: NAO AS A PREDICTOR OF NHT VARIABILITY. *Geophys.*
651 *Res. Lett.*, **40**, 5497–5502, doi:10.1002/2013GL057877.

652 Lohmann, K., H. Drange, and M. Bentsen, 2009: Response of the North Atlantic subpolar gyre to
653 persistent North Atlantic oscillation like forcing. *Clim. Dyn.*, **32**, 273–285, doi:10.1007/s00382-
654 008-0467-6.

655 Magnusson, L., M. Alonso-Balmaseda, and F. Molteni, 2013: On the dependence of ENSO simulation on
656 the coupled model mean state. *Clim. Dyn.*, **41**, 1509–1525, doi:10.1007/s00382-012-1574-y.

657 McCarthy, G. D., I. D. Haigh, J. J.-M. Hirschi, J. P. Grist, and D. A. Smeed, 2015: Ocean impact on decadal
658 Atlantic climate variability revealed by sea-level observations. *Nature*, **521**, 508–510,
659 doi:10.1038/nature14491.

660 Medhaug, I., H. R. Langehaug, T. Eldevik, T. Furevik, and M. Bentsen, 2012: Mechanisms for decadal
661 scale variability in a simulated Atlantic meridional overturning circulation. *Clim. Dyn.*, **39**, 77–
662 93, doi:10.1007/s00382-011-1124-z.

663 Menary, M. B., W. Park, K. Lohmann, M. Vellinga, M. D. Palmer, M. Latif, and J. H. Jungclaus, 2012: A
664 multimodel comparison of centennial Atlantic meridional overturning circulation variability.
665 *Clim. Dyn.*, **38**, 2377–2388, doi:10.1007/s00382-011-1172-4.

666 Milly, P. C. D., and Coauthors, 2014: An Enhanced Model of Land Water and Energy for Global
667 Hydrologic and Earth-System Studies. *J. Hydrometeorol.*, **15**, 1739–1761, doi:10.1175/JHM-D-
668 13-0162.1.

669 Moore, G. W. K., I. A. Renfrew, and R. S. Pickart, 2013: Multidecadal Mobility of the North Atlantic
670 Oscillation. *J. Clim.*, **26**, 2453–2466, doi:10.1175/JCLI-D-12-00023.1.

671 Park, W., and M. Latif, 2008: Multidecadal and multicentennial variability of the meridional
672 overturning circulation. *Geophys. Res. Lett.*, **35**, doi:10.1029/2008GL035779.
673 http://doi.wiley.com/10.1029/2008GL035779 (Accessed April 28, 2015).

674 Rayner, N. A., D. E. Parker, E. B. Horton, Folland, C.K., Alexander, L.V., and Rowell, D.P., 2003: Global
675 analyses of sea surface temperature, sea ice, and night marine air temperature since the late
676 nineteenth century. *J. Geophys. Res.*, **108**, doi:10.1029/2002JD002670.
677 http://doi.wiley.com/10.1029/2002JD002670 (Accessed September 3, 2014).

678 Roberts, C. D., and Coauthors, 2013: Atmosphere drives recent interannual variability of the Atlantic
679 meridional overturning circulation at 26.5°N: ATMOSPHERE DRIVES AMOC VARIABILITY.
680 *Geophys. Res. Lett.*, **40**, 5164–5170, doi:10.1002/grl.50930.

681 Scaife, A. A., C. K. Folland, L. V. Alexander, A. Moberg, and J. R. Knight, 2008: European Climate
682 Extremes and the North Atlantic Oscillation. *J. Clim.*, **21**, 72–83, doi:10.1175/2007JCLI1631.1.

683 Steinman, B. A., M. E. Mann, and S. K. Miller, 2015: Atlantic and Pacific multidecadal oscillations and
684 Northern Hemisphere temperatures. *Science*, **347**, 988–991, doi:10.1126/science.1257856.

685 Sutton, R., and D. Hodson, 2005: Atlantic Ocean Forcing of North American and European Summer
686 Climate. *Science*, **309**, 115–118.

687 Sutton, R. T., and B. Dong, 2012: Atlantic Ocean influence on a shift in European climate in the 1990s.
688 *Nat. Geosci.*, **5**, 788–792, doi:10.1038/ngeo1595.

689 Trigo, R. M., T. J. Osborn, J. M. Corte-Real, and others, 2002: The North Atlantic Oscillation influence on
690 Europe: climate impacts and associated physical mechanisms. *Clim. Res.*, **20**, 9–17.

691 Tulloch, R., and J. Marshall, 2012: Exploring Mechanisms of Variability and Predictability of Atlantic
692 Meridional Overturning Circulation in Two Coupled Climate Models. *J. Clim.*, **25**, 4067–4080,
693 doi:10.1175/JCLI-D-11-00460.1.

694 Vecchi, G. A., and Coauthors, 2014: On the Seasonal Forecasting of Regional Tropical Cyclone Activity.
695 *J. Clim.*, **27**, 7994–8016, doi:10.1175/JCLI-D-14-00158.1.

696 Vellinga, M., and P. Wu, 2004: Low-latitude freshwater influence on centennial variability of the
697 Atlantic thermohaline circulation. *J. Clim.*, **17**, 4498–4511.

698 Visbeck, M., H. Cullen, G. Krahmann, and N. Naik, 1998: An ocean model's response to North Atlantic
699 Oscillation-like wind forcing. *Geophys. Res. Lett.*, **25**, 4521–4524.

700 Yeager, S., and G. Danabasoglu, 2012: Sensitivity of Atlantic Meridional Overturning Circulation
701 Variability to Parameterized Nordic Sea Overflows in CCSM4. *J. Clim.*, **25**, 2077–2103,
702 doi:10.1175/JCLI-D-11-00149.1.

703 Zhang, R., and G. K. Vallis, 2007: The Role of Bottom Vortex Stretching on the Path of the North
704 Atlantic Western Boundary Current and on the Northern Recirculation Gyre. *J. Phys. Oceanogr.*,
705 **37**, 2053–2080, doi:10.1175/JPO3102.1.

706 ——, T. L. Delworth, and I. M. Held, 2007: Can the Atlantic Ocean drive the observed multidecadal
707 variability in Northern Hemisphere mean temperature? *Geophys. Res. Lett.*, **34**,
708 doi:10.1029/2006GL028683. http://doi.wiley.com/10.1029/2006GL028683 (Accessed May
709 29, 2015).

Zhu, X., and J. Jungclaus, 2008: Interdecadal variability of the meridional overturning circulation as an ocean internal mode. *Clim. Dyn.*, **31**, 731–741, doi:10.1007/s00382-008-0383-9.

Figures

Figure 1 Spatial pattern of the heat flux anomalies (W m^{-2}) used as anomalous flux forcings in the model experiments. The fluxes in the top panel are derived from the ECMWF-Interim reanalysis, and are the mean fluxes over Dec-March that correspond to a one standard deviation anomaly of the North Atlantic Oscillation. The fluxes in the bottom panel are from a long control simulation of the CM2.1 model, and also correspond to a one standard deviation anomaly of the North Atlantic Oscillation. Negative values mean a flux of heat from the ocean to the atmosphere.

Figure 2 (a)-(c) Streamfunction of long-term mean AMOC from various model, units in Sverdrups (1 Sv = 10^6 m^3s^{-1}). (a) CM2.1, (b) FLOR, and (c) FLOR_FA. Flow is proportional to the gradient of the streamfunction, and is clockwise around the contours in the latitude-depth plane. (d) Spectra of the time series of AMOC amplitude in the three models. Black indicates CM2.1, red indicates FLOR, and blue indicates FLOR_FA. For each model the thick line represents the spectral estimates, the thin solid line is a red noise (first order Markov process) spectrum fitted to the model spectrum, and the dashed lines represent 95% confidence interval above the red noise spectrum. The units are frequency along the bottom axis (yr^{-1}) and period in years along the top x-axis. The units along the y-axis are spectral density.

731 Figure 3 Response of the AMOC at 45^{o}N in the CM2.1 model to the switch-on of NAO-related surface
732 heat fluxes in the North Atlantic. The NAO fluxes are switched on at time 0. The quantity plotted is the
733 AMOC in the experiment with the NAO forcing minus the time-mean AMOC in the control simulation.
734
735 Figure 4 Adjustment of the model North Atlantic to a sudden switch on of heat flux anomaly
736 corresponding to a one standard deviation increase of the North Atlantic Oscillation. Top row:
737 Climatological mean fields for various quantities as noted by labels at the top of each column. Rows 2-
738 5: anomalies at various times after the switch on of the heat fluxes. The time is shown on the right,
739 and indicates how much time has passed since the switch on of the NAO-related heat flux forcing. The
740 variables are listed along the top, so that each column corresponds to one variable.
741 Figure 5 Time series of AMOC index (defined as the maximum streamfunction value each year over
742 the domain 20^{o}N-65^{o}N) for various experiments using the CM2.1 model. The red curve in each panel
743 shows values from the reference control simulation, calculated as the ensemble mean over ten
744 segments of the control simulation that correspond to the ten ensemble members of the perturbation
745 experiments. (a) Black (blue) curve shows 10-member ensemble mean AMOC from simulations with
746 NAO forcing at a timescale of 2 (5) years. (b) Black (blue) curve shows 10-member ensemble mean
747 AMOC from simulations with NAO forcing at a timescale of 10 (20) years. (c) Black (blue) curve shows
748 10-member ensemble mean AMOC from simulations with NAO forcing at a timescale of 50 (100)
749 years.
750
751 Figure 6 (a) Each circle represents the standard deviation of the ensemble mean AMOC time series
752 from a perturbation experiment using NAO forcing at a particular timescale. The values along the y-
753 axis indicate the value of the standard deviation, while the values along the x-axis indicate the

timescale (in years) of the NAO forcing for each experiment. (b) Same as (a) for meridional ocean heat transport at 23^{o}N (summed over all longitudes, units are 10^{15} W). (c) Same as (a) for annual mean surface air temperature (units are K) averaged over all points poleward of 23^{o}N. (d) Same as (a) for annual mean sea ice thickness averaged over all points poleward of 55^{o}N, units are cm. (e) Same as (a) for air-sea surface heat flux averaged over all points poleward of 23^{o}N, units are W m^{-2}. (f) Same as (a) for net upward shortwave radiation at the top of the atmosphere, averaged over all points poleward of 23^{o}N, units are W m^{-2}.

Figure 7 Time series of various quantities in model simulations driven by a periodic NAO heat flux forcing. In each panel we show the results from a 20-year timescale NAO forcing experiment (black) and a 100-year timescale NAO forcing (red). Each time series is the 10-member ensemble mean of the NAO forced experiment minus the corresponding control simulation. The 20-year (100-year) forcing experiments are 100 (200) years in duration. (a) AMOC index, units are Sv. (b) Meridional ocean heat transport at 23^{o}N, units are 10^{15} W. (c) Surface air temperature, averaged over all points poleward of 23^{o}N, units are K. (d) Annual mean sea ice thickness, averaged over all points poleward of 55^{o}N, units are c,. (e) Annual mean net upward shortwave radiation at the top of the atmosphere (W m^{-2}), averaged over all points poleward of 23^{o}N. (f) Ocean-atmosphere heat flux (W m^{-2}), averaged over all points poleward of 23^{o}N.

Figure 8 Spatial patterns of simulated response to an increase in the AMOC induced NAO-related surface heat flux anomalies. The responses are averaged over the months of Jan-Mar. Left (right) column shows results from simulations with 20-year (100-year) NAO forcing. Values plotted are regression coefficients of the various fields versus the time series of the heat flux forcing; these are

normalized to represent the response to a two standard deviation change in the NAO-induced fluxes. Left column are results for a 20-year timescale of flux forcing, showing fields 7 years after maximum of imposed NAO flux forcing. The right column shows results for a 100-year timescale of flux forcing, plotted 13 years after maximum of imposed NAO flux forcing.

Figure 9 Spatial patterns of simulated response of sea ice thickness to NAO heat fluxes, with the responses averaged over the months of Jan-Mar. Units for sea ice thickness are meters per two standard deviation NAO forcing.

Figure 10 Spatial patterns of simulated response to an increase in the AMOC induced by NAO-related surface heat flux anomalies. The responses are averaged over the months of Jul-Sep. Left (right) column shows results from simulations with 20-year (100-year) NAO forcing. Values plotted are regression coefficients of the various fields versus the time series of the heat flux forcing; these are normalized to represent the response to a two standard deviation change in the NAO-induced fluxes. Left column are results for a 20-year timescale of flux forcing, showing fields 7 years after maximum of imposed NAO flux forcing. The right column shows results for a 100-year timescale of flux forcing, plotted 13 years after maximum of imposed NAO flux forcing. The vertical shear of the zonal wind (bottom row) is calculated as the zonal wind at 250 hPa minus the zonal wind at 850 hPa.

Figure 11 Spatial patterns of simulated response of sea ice thickness to NAO heat fluxes, with the responses averaged over the months of Jul-Sep.

Figure 12 Regression of annual mean sea level height anomaly versus the time series of NAO forcing, expressed as the difference in cm between a positive one standard deviation NAO forcing and a negative one standard deviation NAO forcing. The maps are representative of conditions 7 years after the maximum NAO flux forcing. (a) Case with NAO-forcing at 20 years. (b) Case with NAO-forcing at 100 years.

Figure 13 Response of AMOC (left column) and zonally averaged surface air temperature (right column) to sudden switch on of NAO related heat flux forcing. Top row is from CM2.1, middle row from FLOR, and bottom row from FLOR_FA. Units are Sv for AMOC changes, and K for temperature changes. Time is listed along the x-axis in years, latitude is on the y-axis.

Figure 14 Response of AMOC (left column) and zonally averaged surface air temperature (right column) to 50-year timescale NAO heat flux forcing. Top row is from CM2.1, middle row from FLOR, and bottom row from FLOR_FA. Units are Sv for AMOC changes, and K for temperature changes. Time is listed along the x-axis in years, and latitude along the y-axis.

Figure 15 Response to 50-year NAO heat flux forcing calculated as the ensemble mean response from CM2.1, FLOR, and FLOR_FA. Top panel shows NH mean surface air temperature, while bottom panel shows the AMOC. Time is listed in years along the x-axis, indicating years since switching on the NAO-related heat fluxes. Units are Sv for AMOC changes, and K for temperature changes.

819

820

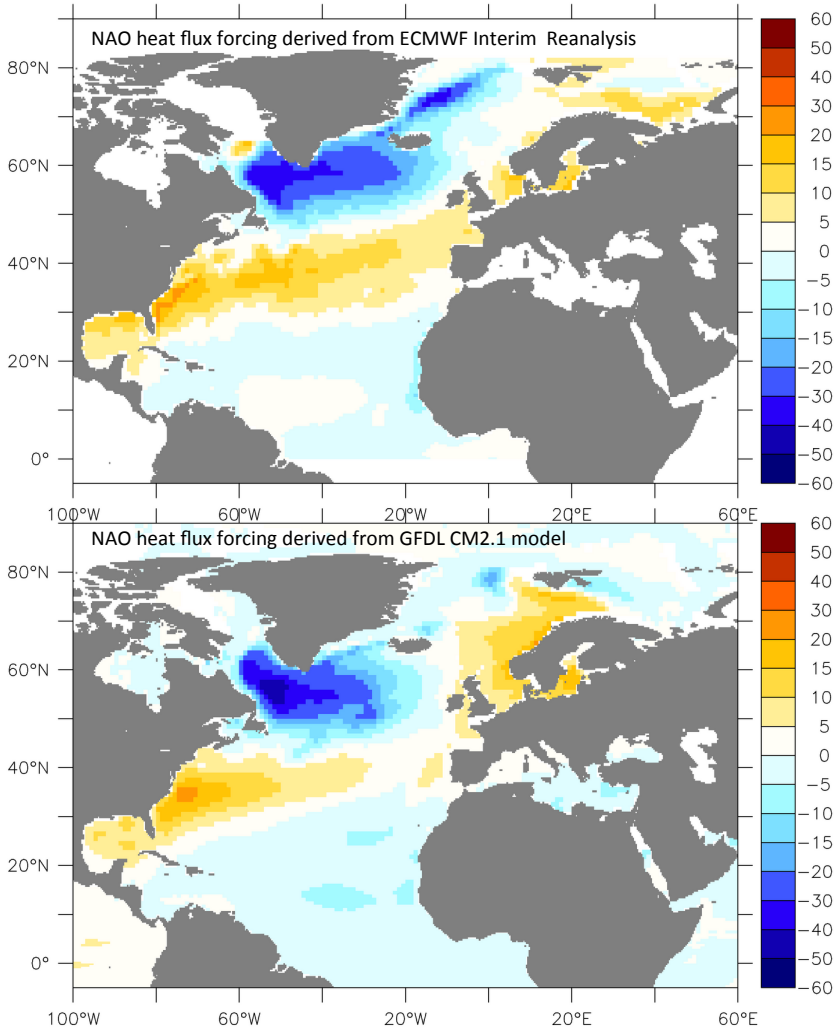

Figure 1 Spatial pattern of the heat flux anomalies (W m^{-2}) used as anomalous flux forcings in the model experiments. The fluxes in the top panel are derived from the ECMWF-Interim reanalysis, and are the mean fluxes over Dec-March that correspond to a one standard deviation anomaly of the North Atlantic Oscillation. The fluxes in the bottom panel are from a long control simulation of the CM2.1 model, and also correspond to a one standard deviation anomaly of the North Atlantic Oscillation. Negative values mean a flux of heat from the ocean to the atmosphere.

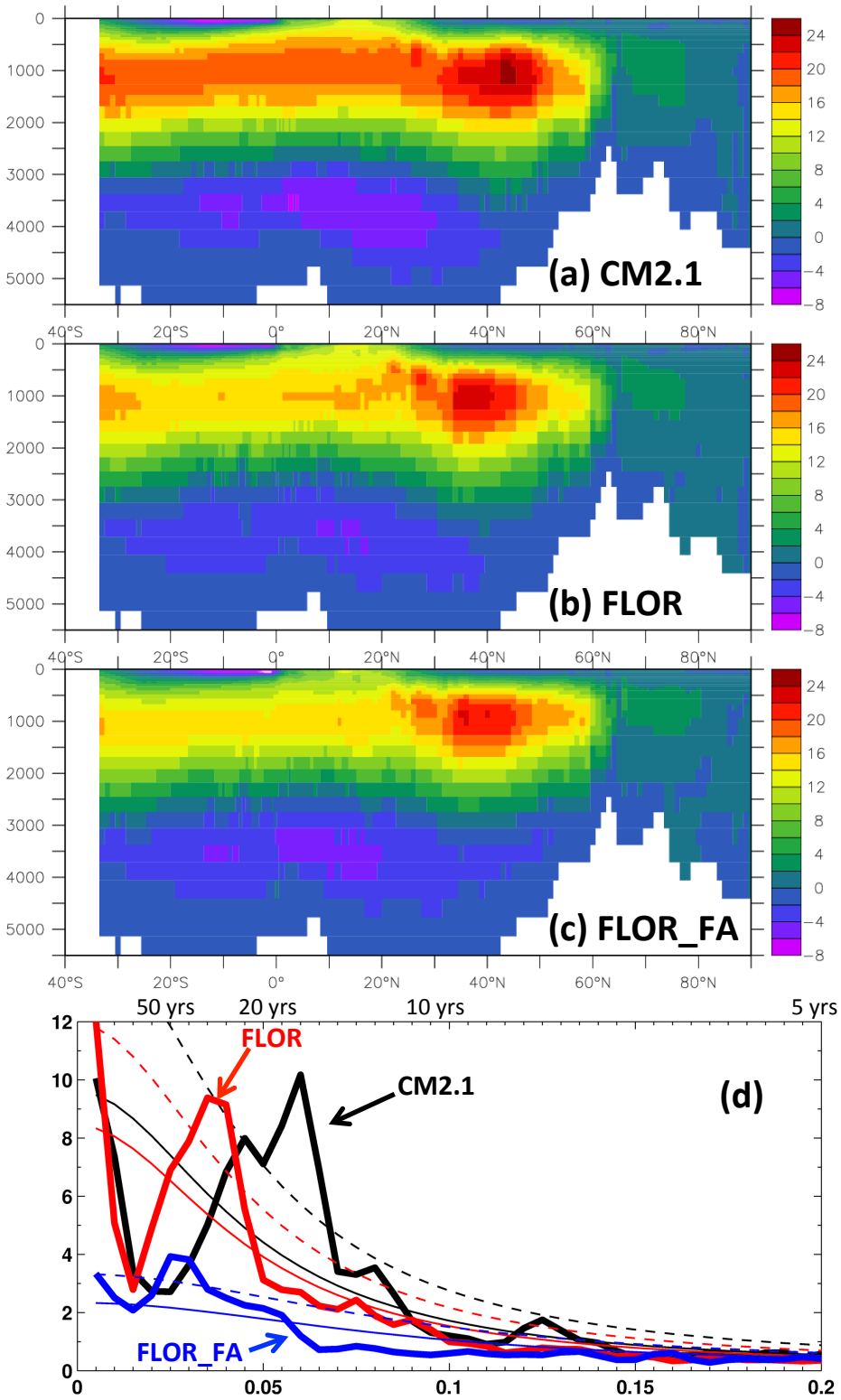

Figure 2 (a)-(c) Streamfunction of long-term mean AMOC from various model, units in Sverdrups (1 Sv = 10^6 m^3s^{-1}). (a) CM2.1, (b) FLOR, and (c) FLOR_FA. Flow is proportional to the gradient of the streamfunction, and is clockwise around the contours in the latitude-depth plane. (d) Spectra of the time series of AMOC amplitude in the three models. Black indicates CM2.1, red indicates FLOR, and blue indicates FLOR_FA. For each model the thick line represents the spectral estimates, the thin solid line is a red noise (first order Markov process) spectrum fitted to the model spectrum, and the dashed lines represent 95% confidence interval above the red noise spectrum. The units are frequency along the bottom axis (yr^{-1}) and period in years along the top x-axis. The units along the y-axis are spectral density.

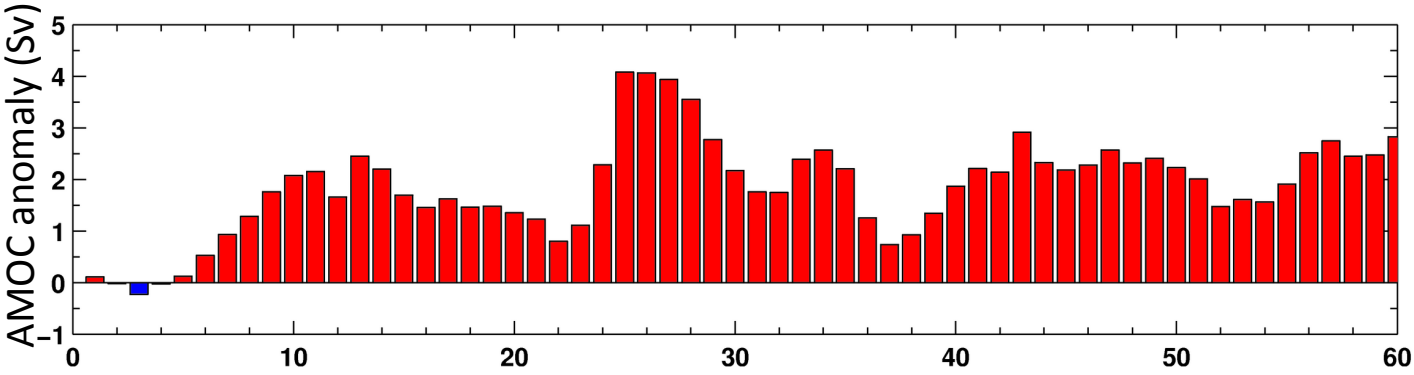

Figure 3 Response of the AMOC at 45°N in the CM2.1 model to the switch-on of NAO-related surface heat fluxes in the North Atlantic. The NAO fluxes are switched on at time 0. The quantity plotted is the AMOC in the experiment with the NAO forcing minus the time-mean AMOC in the control simulation.

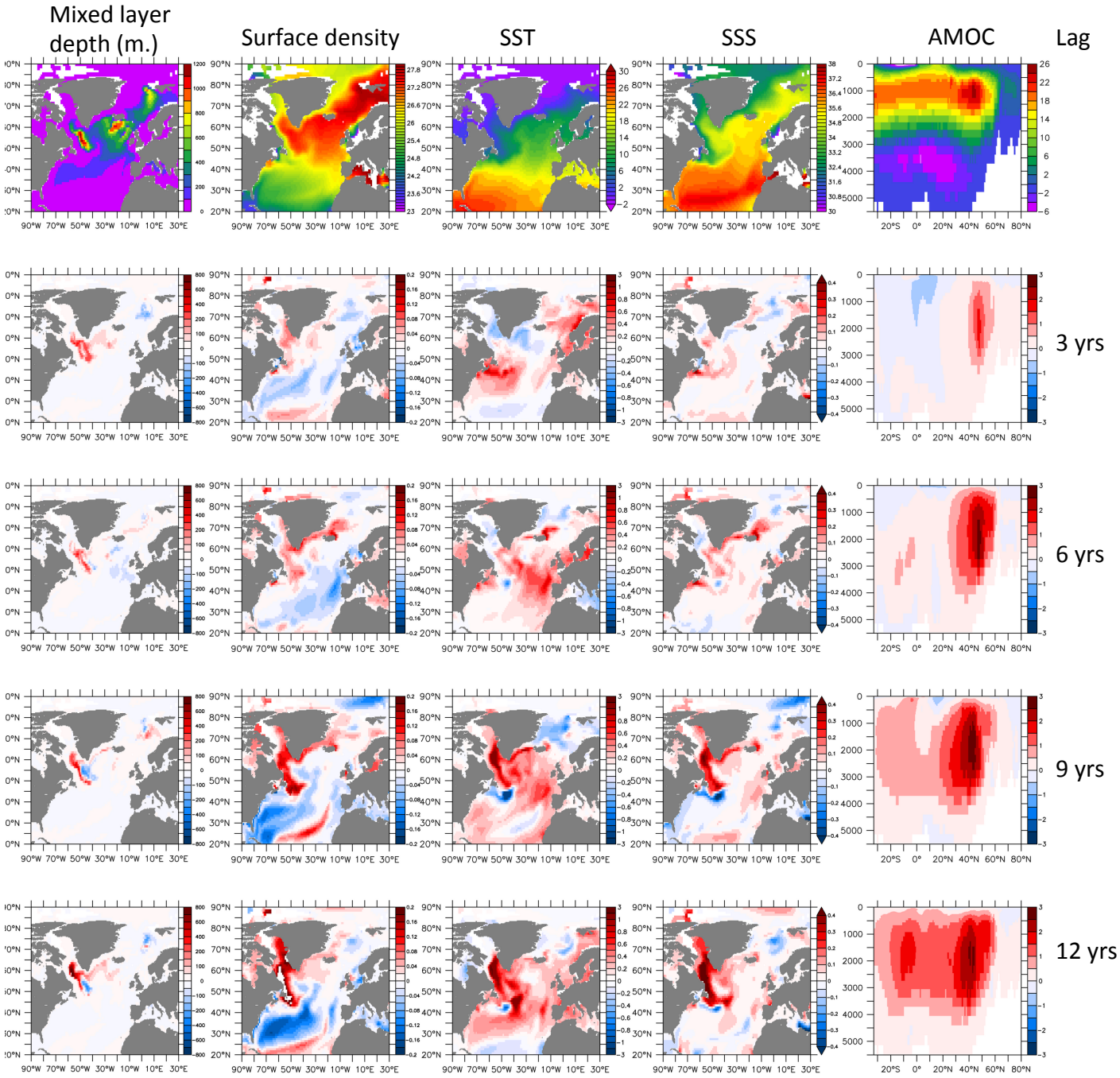

Figure 4 Adjustment of the model North Atlantic to a sudden switch on of heat flux anomaly corresponding to a one standard deviation increase of the North Atlantic Oscillation. Top row: Climatological mean fields for various quantities as noted by labels at the top of each column. Rows 2-5: anomalies at various times after the switch on of the heat fluxes. The time is shown on the right, and indicates how much time has passed since the switch on of the NAO-related heat flux forcing. The variables are listed along the top, so that each column corresponds to one variable.

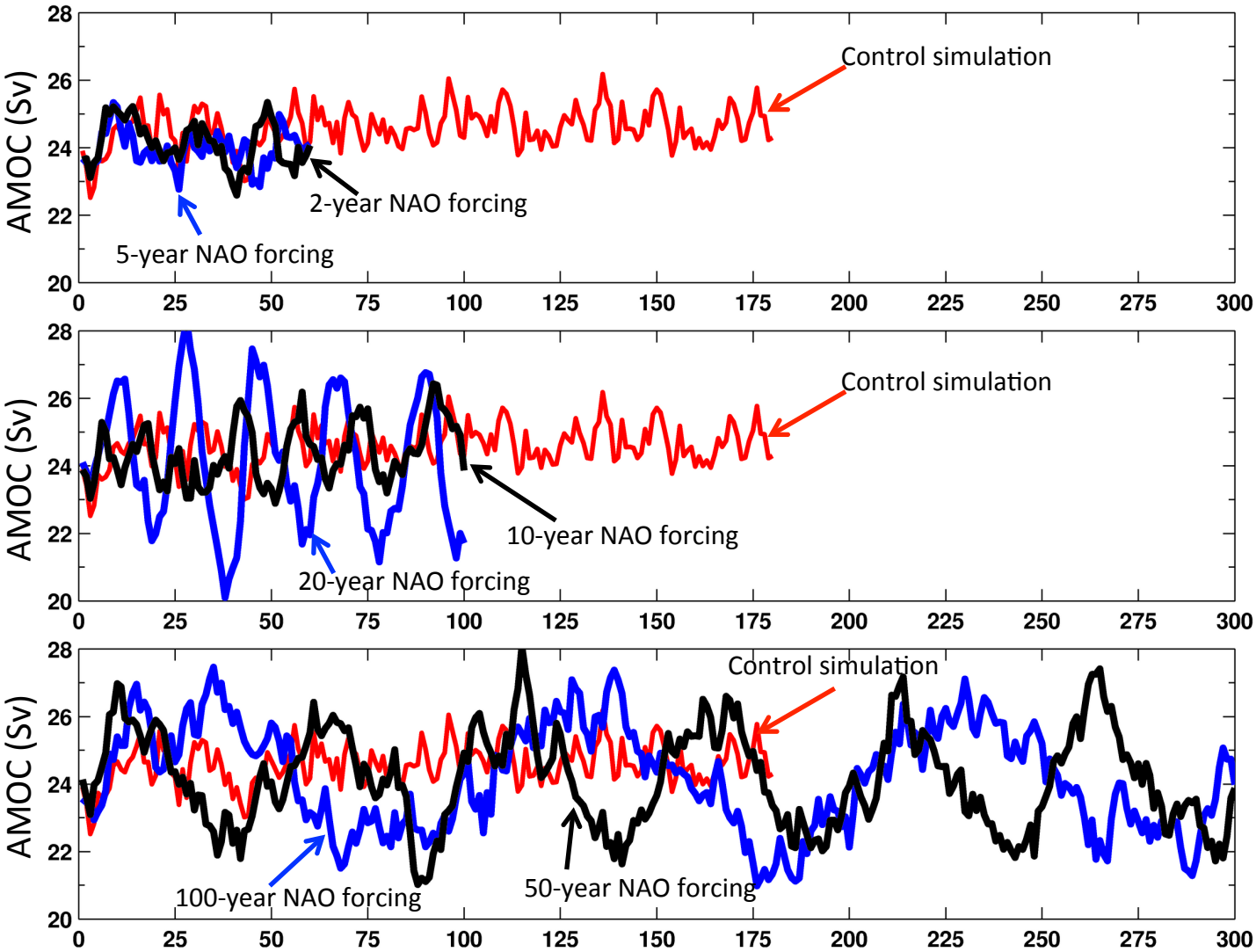

Figure 5 Time series of AMOC index (defined as the maximum streamfunction value each year over the domain 20°N-65°N) for various experiments using the CM2.1 model. The red curve in each panel shows values from the reference control simulation, calculated as the ensemble mean over ten segments of the control simulation that correspond to the ten ensemble members of the perturbation experiments. (a) Black (blue) curve shows 10-member ensemble mean AMOC from simulations with NAO forcing at a timescale of 2 (5) years. (b) Black (blue) curve shows 10-member ensemble mean AMOC from simulations with NAO forcing at a timescale of 10 (20) years. (c) Black (blue) curve shows 10-member ensemble mean AMOC from simulations with NAO forcing at a timescale of 50 (100) years.

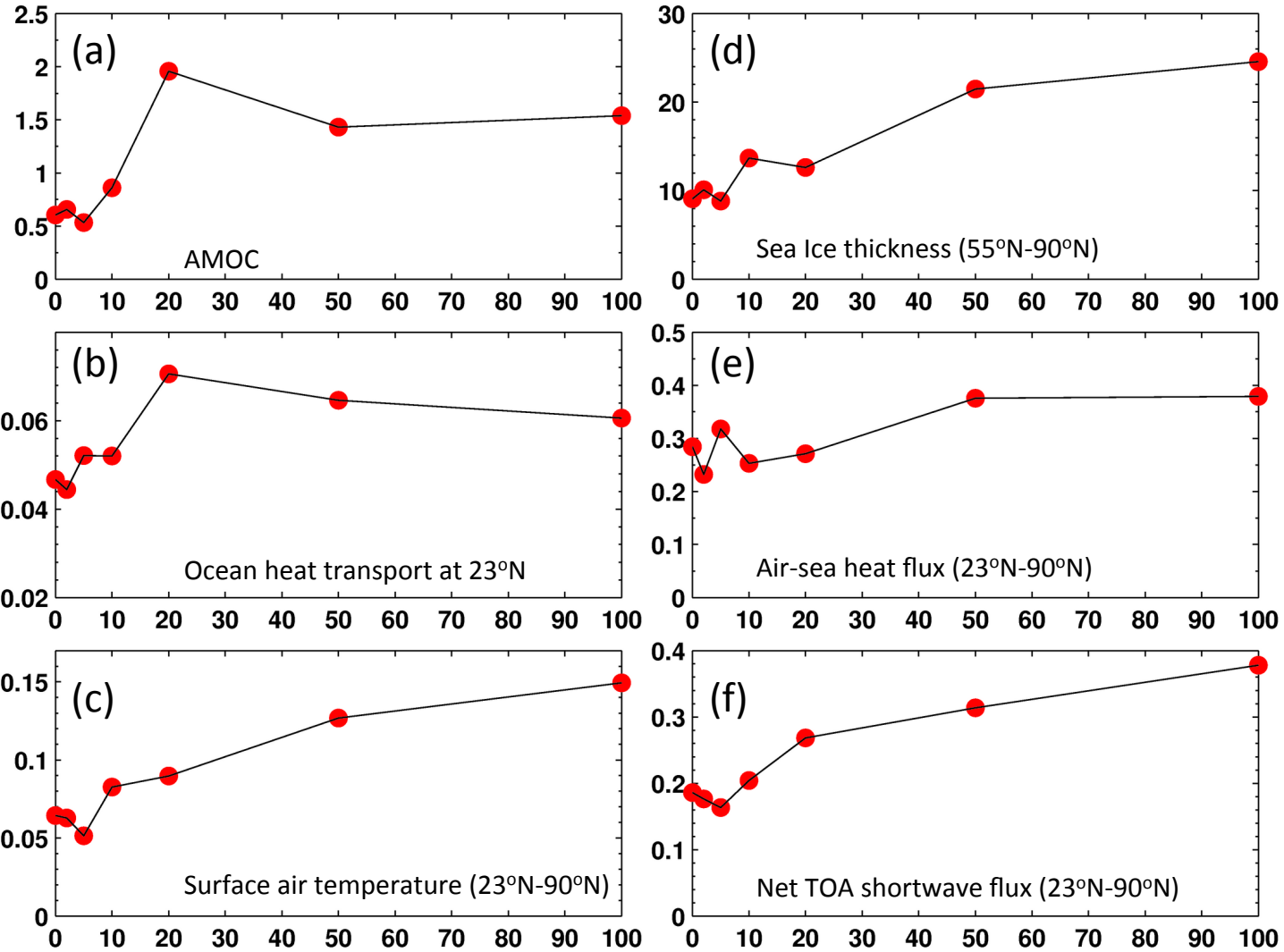

Figure 6 (a) Each circle represents the standard deviation of the ensemble mean AMOC time series from a perturbation experiment using NAO forcing at a particular timescale. The values along the y-axis indicate the value of the standard deviation, while the values along the x-axis indicate the timescale (in years) of the NAO forcing for each experiment. (b) Same as (a) for meridional ocean heat transport at 23°N (summed over all longitudes, units are 10^{15} W). (c) Same as (a) for annual mean surface air temperature (units are K) averaged over all points poleward of 23°N. (d) Same as (a) for annual mean sea ice thickness averaged over all points poleward of 55°N, units are cm. (e) Same as (a) for air-sea surface heat flux averaged over all points poleward of 23°N, units are W m^{-2}. (f) Same as (a) for net upward shortwave radiation at the top of the atmosphere, averaged over all points poleward of 23°N, units are W m^{-2}.

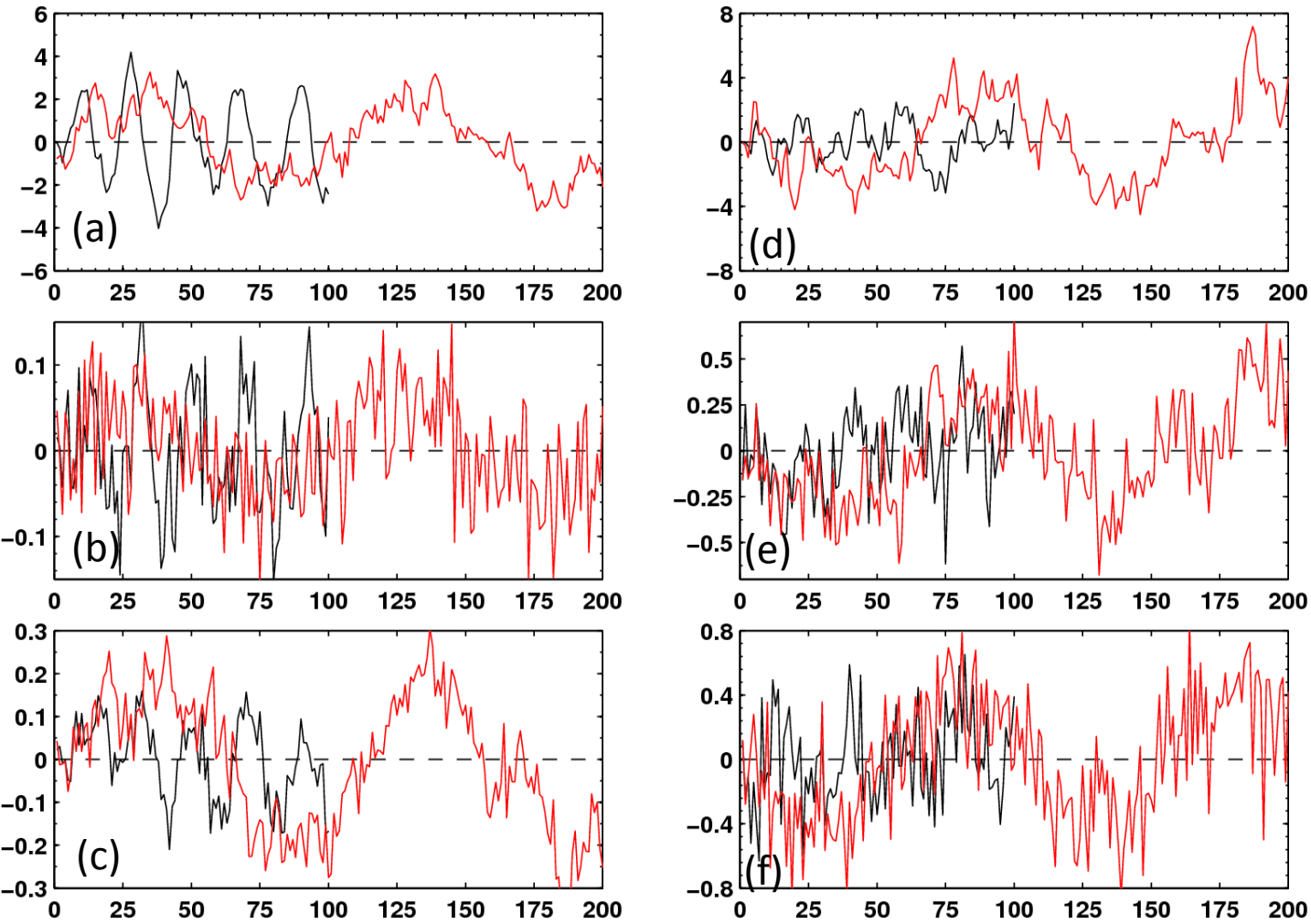

Figure 7 Time series of various quantities in model simulations driven by a periodic NAO heat flux forcing. In each panel we show the results from a 20-year timescale NAO forcing experiment (black) and a 100-year timescale NAO forcing (red). Each time series is the 10-member ensemble mean of the NAO forced experiment minus the corresponding control simulation. The 20-year (100-year) forcing experiments are 100 (200) years in duration. (a) AMOC index, units are Sv. (b) Meridional ocean heat transport at 23^{o}N, units are 10^{15} W. (c) Surface air temperature, averaged over all points poleward of 23^{o}N, units are K. (d) Annual mean sea ice thickness, averaged over all points poleward of 55^{o}N, units are c,. (e) Annual mean net upward shortwave radiation at the top of the atmosphere (W m^{-2}), averaged over all points poleward of 23^{o}N. (f) Ocean-atmosphere heat flux (W m^{-2}), averaged over all points poleward of 23^{o}N.

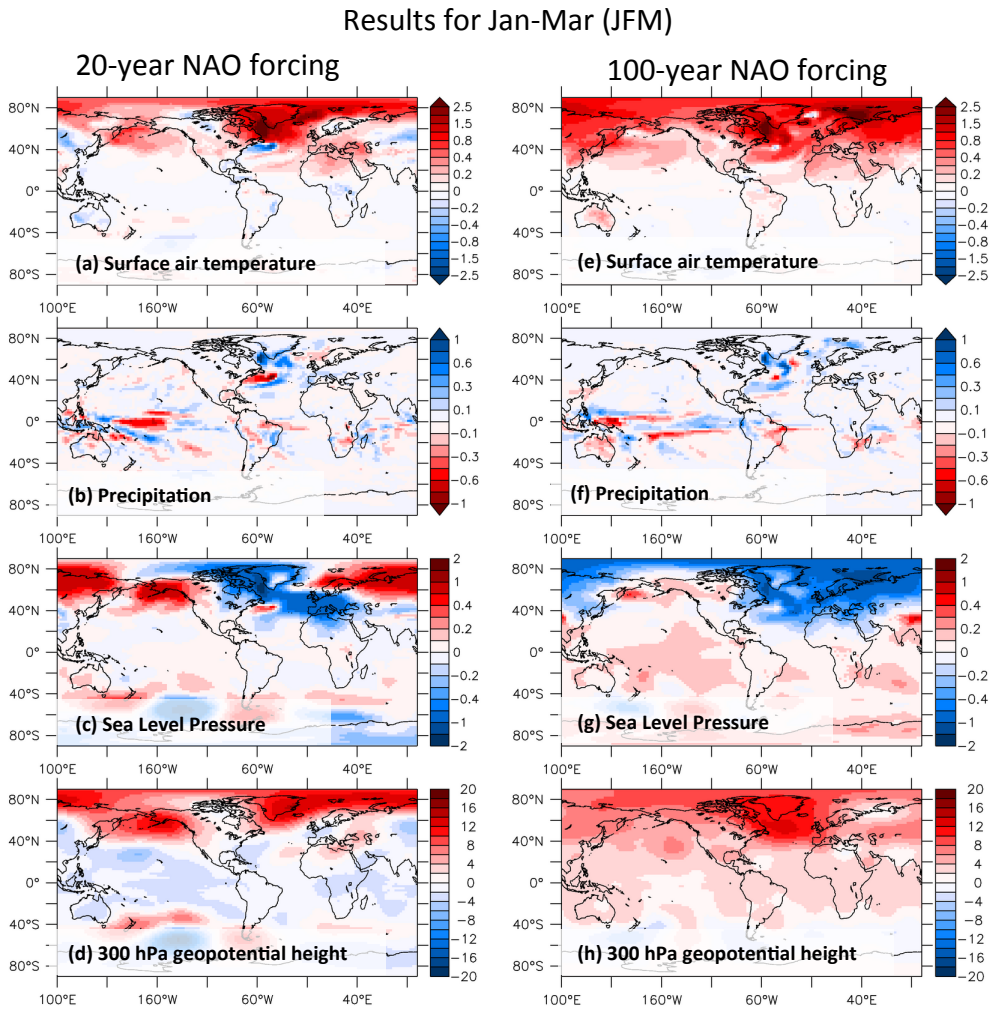

Figure 8 Spatial patterns of simulated response to an increase in the AMOC induced NAO-related surface heat flux anomalies. The responses are averaged over the months of Jan-Mar. Left (right) column shows results from simulations with 20-year (100-year) NAO forcing. Values plotted are regression coefficients of the various fields versus the time series of the heat flux forcing; these are normalized to represent the response to a two standard deviation change in the NAO-induced fluxes. Left column are results for a 20-year timescale of flux forcing, showing fields 7 years after maximum of imposed NAO flux forcing. The right column shows results for a 100-year timescale of flux forcing, plotted 13 years after maximum of imposed NAO flux forcing.

Results for Jan-Mar (JFM)

20-year NAO forcing

100-year NAO forcing

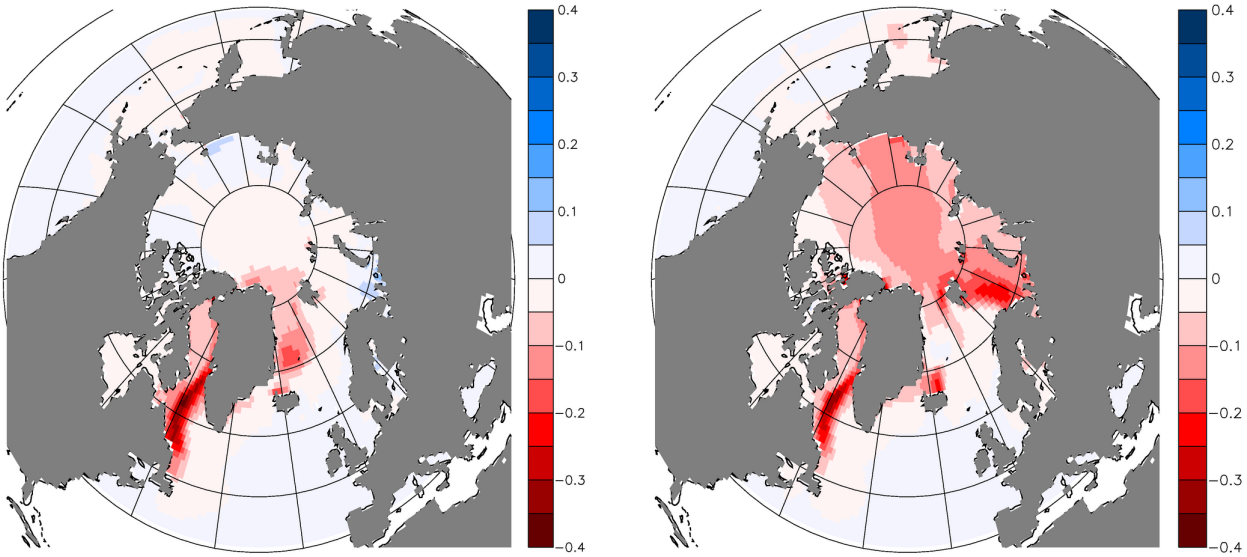

Figure 9 Spatial patterns of simulated response of sea ice thickness to NAO heat fluxes, with the responses averaged over the months of Jan-Mar. Units for sea ice thickness are meters per two standard deviation NAO forcing.

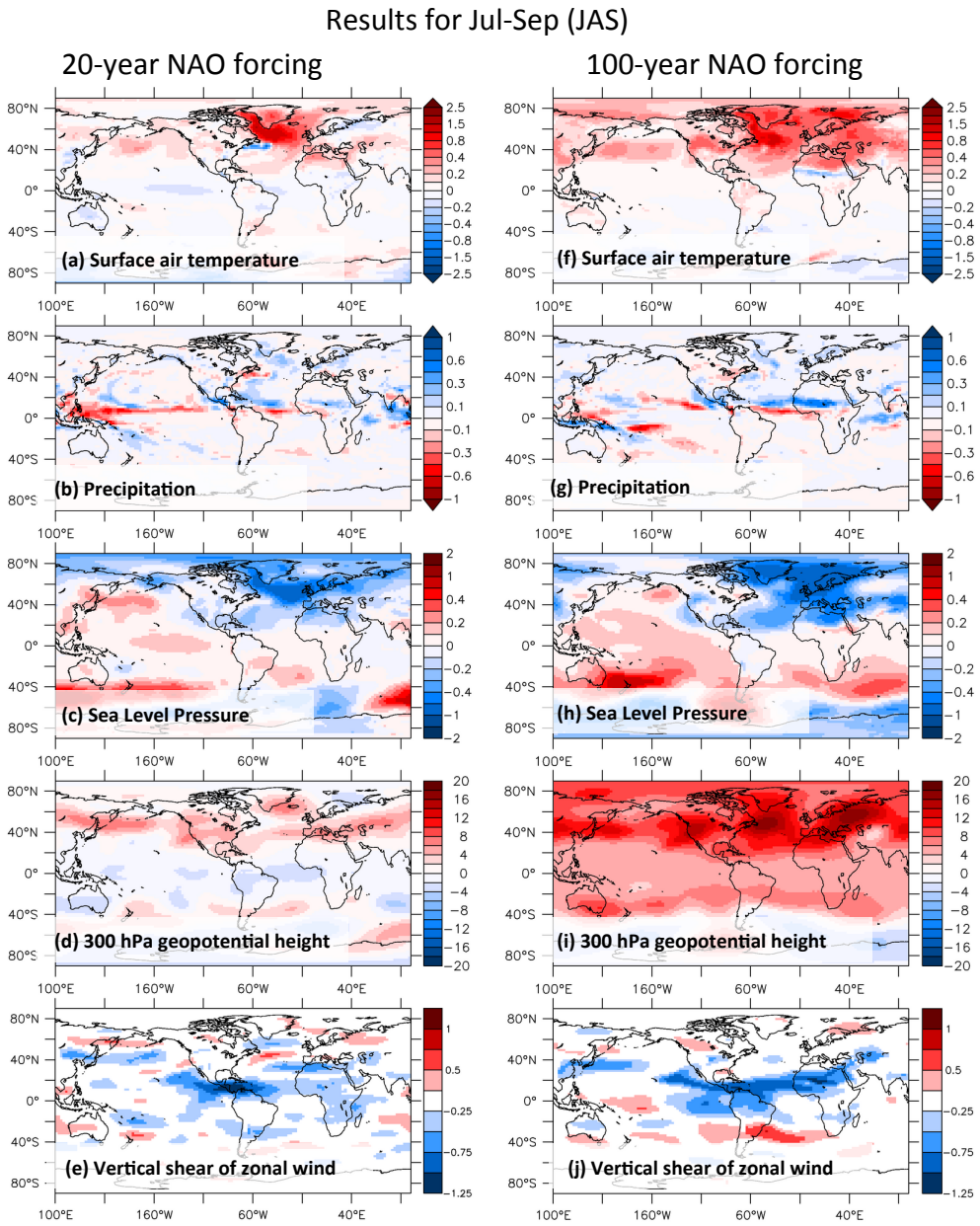

Figure 10 Spatial patterns of simulated response to an increase in the AMOC induced by NAO-related surface heat flux anomalies. The responses are averaged over the months of Jul-Sep. Left (right) column shows results from simulations with 20-year (100-year) NAO forcing. Values plotted are regression coefficients of the various fields versus the time series of the heat flux forcing; these are normalized to represent the response to a two standard deviation change in the NAO-induced fluxes. Left column are results for a 20-year timescale of flux forcing, showing fields 7 years after maximum of imposed NAO flux forcing. The right column shows results for a 100-year timescale of flux forcing, plotted 13 years after maximum of imposed NAO flux forcing. The vertical shear of the zonal wind (bottom row) is calculated as the zonal wind at 250 hPa minus the zonal wind at 850 hPa.

Results for Jul-Sep (JAS)

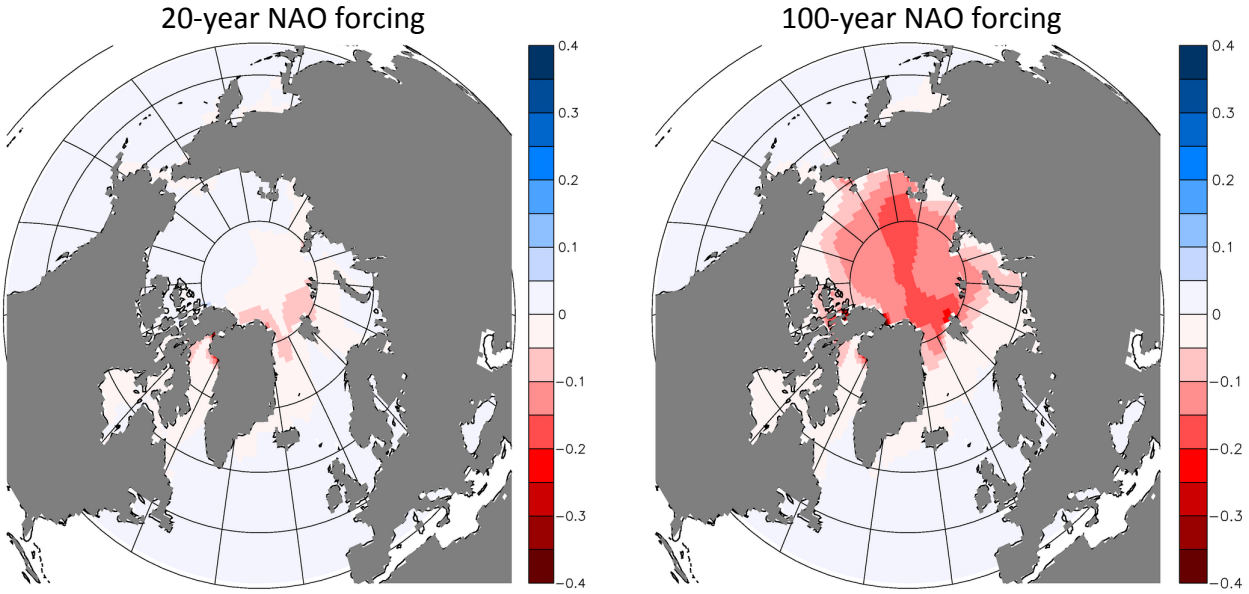

Figure 11 Spatial patterns of simulated response of sea ice thickness to NAO heat fluxes, with the responses averaged over the months of Jul-Sep.

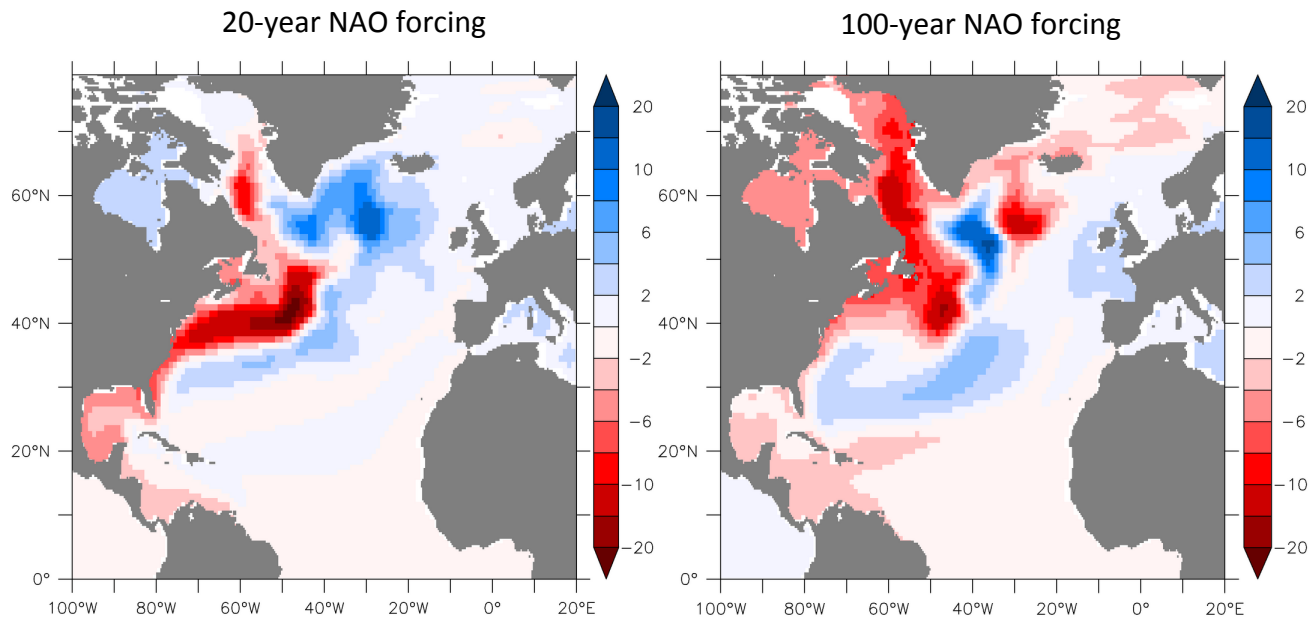

Figure 12 Regression of annual mean sea level height anomaly versus the time series of NAO forcing, expressed as the difference in cm between a positive one standard deviation NAO forcing and a negative one standard deviation NAO forcing. The maps are representative of conditions 7 years after the maximum NAO flux forcing. (a) Case with NAO-forcing at 20 years. (b) Case with NAO-forcing at 100 years.

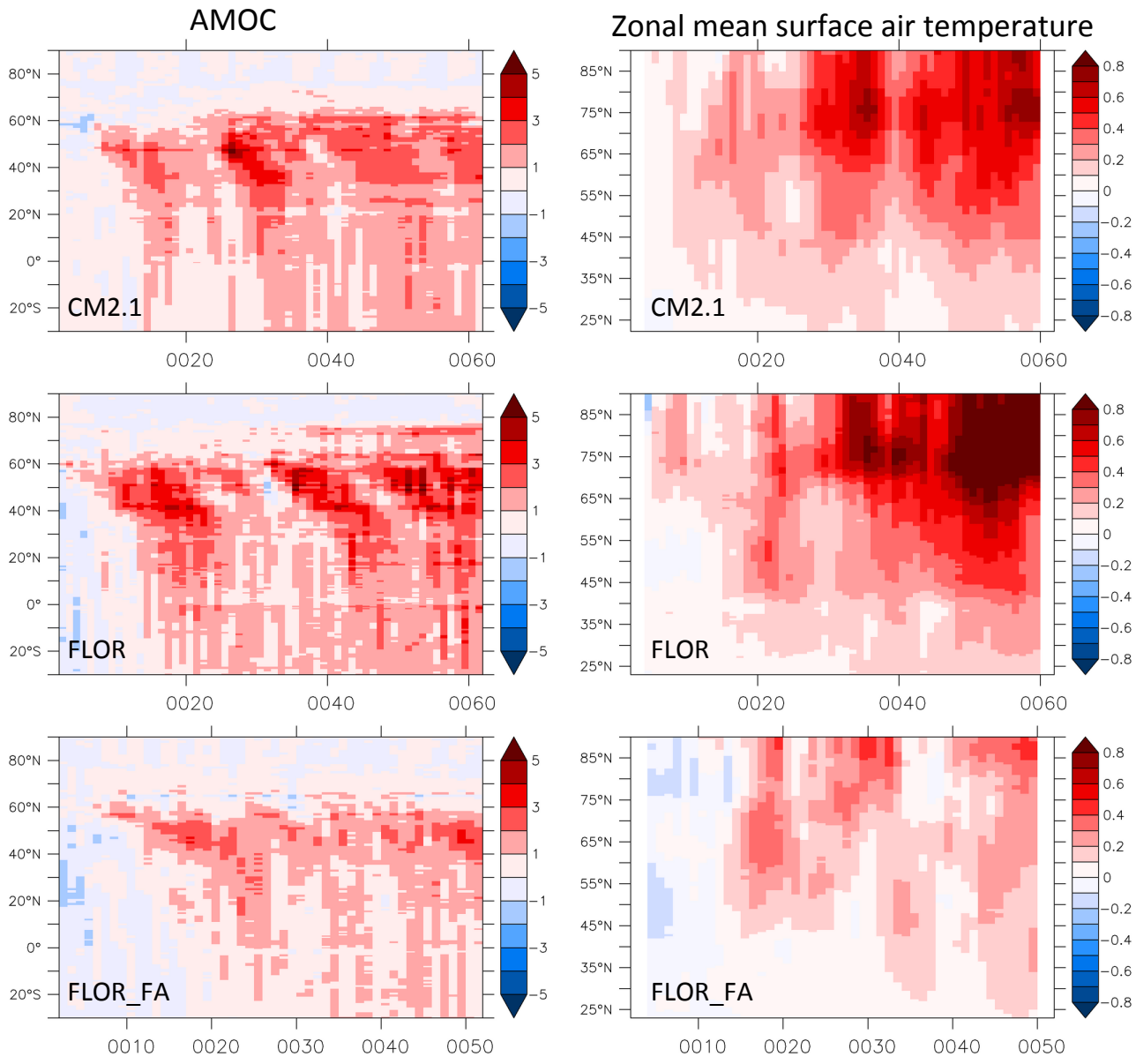

Figure 13 Response of AMOC (left column) and zonally averaged surface air temperature (right column) to sudden switch on of NAO related heat flux forcing. Top row is from CM2.1, middle row from FLOR, and bottom row from FLOR_FA. Units are Sv for AMOC changes, and K for temperature changes. Time is listed along the x-axis in years, latitude is on the y-axis.

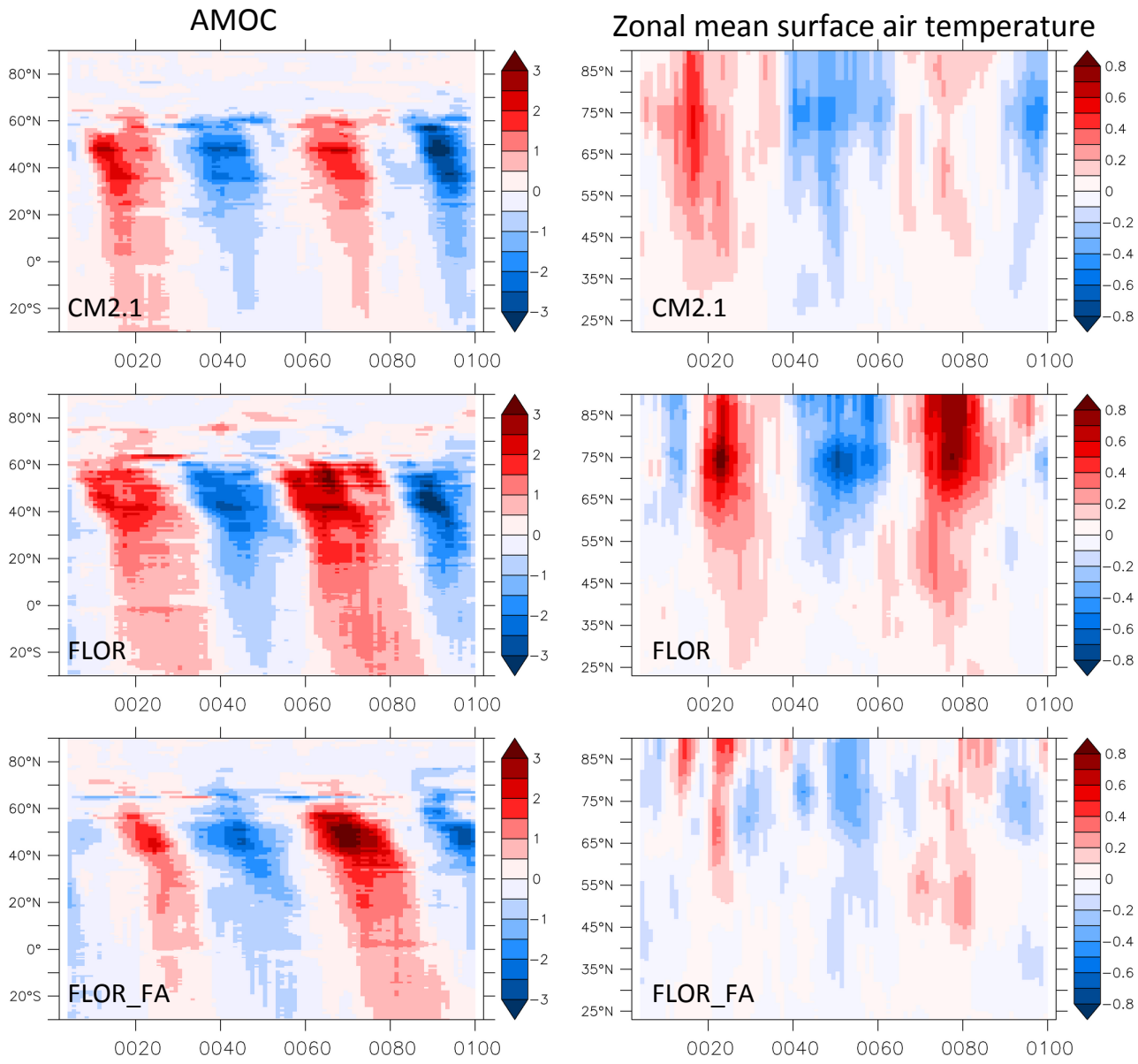

Figure 14 Response of AMOC (left column) and zonally averaged surface air temperature (right column) to 50-year timescale NAO heat flux forcing. Top row is from CM2.1, middle row from FLOR, and bottom row from FLOR_FA. Units are Sv for AMOC changes, and K for temperature changes. Time is listed along the x-axis in years, and latitude along the y-axis.

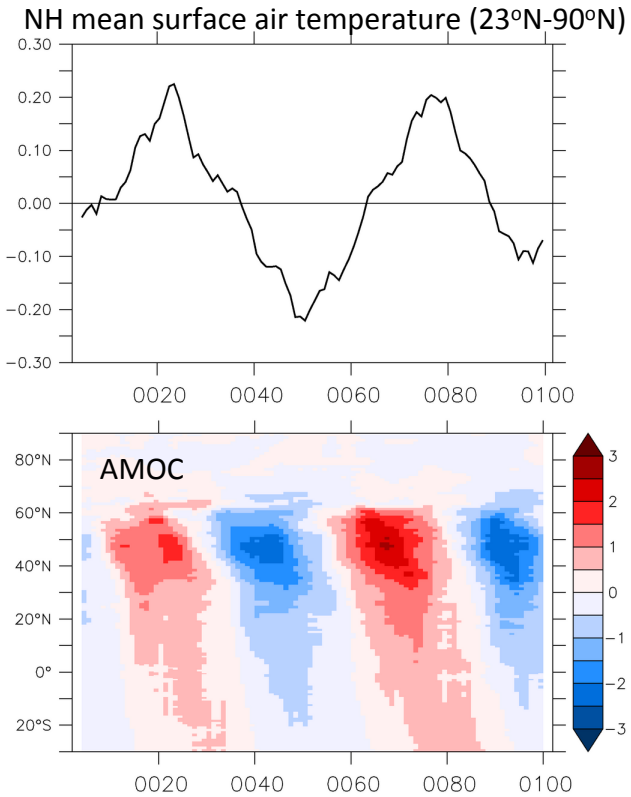

Figure 15 Response to 50-year NAO heat flux forcing calculated as the ensemble mean response from CM2.1, FLOR, and FLOR_FA. Top panel shows NH mean surface air temperature, while bottom panel shows the AMOC. Time is listed in years along the x-axis, indicating years since switching on the NAO-related heat fluxes. Units are Sv for AMOC changes, and K for temperature changes.